Cell Metabolism

DELETION OR INHIBITION OF THE OXYGEN SENSOR PHD1 PROTECTS AGAINST ISCHEMIC STROKE VIA REPROGRAMMING OF NEURONAL METABOLISM

--Manuscript Draft--

Manuscript Number:	CELL-METABOLISM-D-14-00600R2
Full Title:	DELETION OR INHIBITION OF THE OXYGEN SENSOR PHD1 PROTECTS AGAINST ISCHEMIC STROKE VIA REPROGRAMMING OF NEURONAL METABOLISM
Article Type:	Research Article
Keywords:	Ischemic stroke; oxygen sensor; neuroprotection; neuronal metabolism; oxidative pentose-phosphate pathway
Corresponding Author:	Peter Carmeliet, MD, PhD VIB Leuven, BELGIUM
First Author:	Annelies Quaegebeur
Order of Authors:	Annelies Quaegebeur
	Inmaculada Segura
	Roberta Schmieder
	Dries Verdegem
	Ilaria Decimo
	Francesco Bifari
	Tom Dresselaers
	Guy Eelen
	Debapriva Ghosh
	Sandra Schoors
	Dorien Broekaert
	Bert Cruys
	Kristof Govaerts
	Carla De Legher
	Ann Bouché
	luc schoonjans
	Matt s Ramer
	Gene Hung
	Goele Bossaert
	Don W. Cleveland
	Uwe Himmelreich
	Thomas Voets
	Robin Lemmens
	C. Frank Bennett
	Robberecht Wim
	Katrien De Bock

	Mieke Dewerchin
	Sarah-Maria Fendt
	Bart Ghesquière
	Peter Carmeliet, MD, PhD
Abstract:	The oxygen-sensing prolyl hydroxylase domain proteins (PHDs) regulate cellular metabolism, but their role in neuronal metabolism during stroke is unknown. Here we report that PHD1 deficiency provides neuroprotection in a murine model of permanent brain ischemia. This was not due to an increased collateral vessel network. Instead, PHD1-/- neurons were protected against oxygen-nutrient deprivation by reprogramming glucose metabolism. Indeed, PHD1-/- neurons enhanced glucose flux through the oxidative pentose phosphate pathway by diverting glucose away from glycolysis. As a result, PHD1-/- neurons increased their redox buffering capacity to scavenge oxygen radicals in ischemia. Intracerebroventricular injection of PHD1-antisense oligonucleotides reduced the cerebral infarct size and neurological deficits following stroke. These data identify PHD1 as a regulator of neuronal metabolism and a potential therapeutic target in ischemic stroke.
Suggested Reviewers:	Berislav V. Zlokovic Berislav.Zlokovic@med.usc.edu expert in cerebrovascular disease and neurobiology, who has been recently studying neuronal metabolism (as presented at international meetings)
	Patrik Verstreken Patrik.Verstreken@cme.vib-kuleuven.be expert in neurobiology and mitochondrial metabolism.
	Celeste Simon celeste2@mail.med.upenn.edu expert in hypoxia signaling (HIFs/PHDs) and metabolism, who has published studies on neurobiology
Opposed Reviewers:	Rajiv Ratan rratan@burke.org
	William G Kaelin william_kaelin@dfci.harvard.edu
	Ray Swanson Raymond.Swanson@ucsf.edu

VIB Vesalius Research Center

Dr. Nikla Emambokus
Editor *Cell Metabolism*
600 Technology Square,
STE 5 Cambridge,
MA 02139,
USA

Leuven, December 3, 2015

Dear Nikla,

Many thanks for your positive editorial decision about our revised manuscript, entitled "Inhibition or deletion of the oxygen sensor PHD1 protects against ischemic stroke via reprogramming of neuronal metabolism" by A. Quaegebeur and co-authors (CELL-METABOLISM-D-14-00600).

We have followed the guidelines of the journal, and made the appropriate changes in the main text and other associated files.

In particular, we addressed the following points:

1) We reduced the length of the manuscript to below 55,000 characters without however changing the scientific content or leaving out data.
2) We have added a graphical abstract illustrating the main message of our work.
3) In our original manuscript, Figure 6 showed an immunoblot of the total p65 levels. Since nuclear p65 levels more accurately reflect the activation status of NF-κB signaling, we replaced the panel showing the total p65 levels with one showing the nuclear p65 levels, and removed the blot of the total p65 levels to Supplementary Figure 5. Like for the total p65, PHD1 deficiency increased the levels of the nuclear p65. This small change thus represents an improvement of these p65 data.
4) Additional supporting grants have been included in the acknowledgment

We hope that you will find our revision satisfactory, and look forward to hearing your response.

Thank you very much for your consideration.

Best personal regards,

Peter Carmeliet

Peter Carmeliet, MD, PhD
Professor of Medicine

KU LEUVEN

VIB - KU Leuven I Vesalius Research Center – Department of Oncology
Campus Gasthuisberg O&N 4 I Herestraat 49 - B 912, 3000 Leuven I
Phone : +32 16 37 32 35 I Fax : +32 16 37 25 85 I www.vrc-lab.be

VIB Vesalius Research Center

Dr. Nikla Emambokus
Editor *Cell Metabolism*
600 Technology Square,
STE 5 Cambridge,
MA 02139,
USA

Leuven, December 3, 2015

Dear Nikla,

Many thanks for your positive editorial decision about our revised manuscript, entitled "Inhibition or deletion of the oxygen sensor PHD1 protects against ischemic stroke via reprogramming of neuronal metabolism" by A. Quaegebeur and co-authors (CELL-METABOLISM-D-14-00600).

We have followed the guidelines of the journal, and made the appropriate changes in the main text and other associated files.

In particular, we addressed the following points:

1) We reduced the length of the manuscript to below 55,000 characters without however changing the scientific content or leaving out data.
2) We have added a graphical abstract illustrating the main message of our work.
3) In our original manuscript, Figure 6 showed an immunoblot of the total p65 levels. Since nuclear p65 levels more accurately reflect the activation status of NF-κB signaling, we replaced the panel showing the total p65 levels with one showing the nuclear p65 levels, and removed the blot of the total p65 levels to Supplementary Figure 5. Like for the total p65, PHD1 deficiency increased the levels of the nuclear p65. This small change thus represents an improvement of these p65 data.
4) Additional supporting grants have been included in the acknowledgment

We hope that you will find our revision satisfactory, and look forward to hearing your response.

Thank you very much for your consideration.

Best personal regards,

Peter Carmeliet

Peter Carmeliet, MD, PhD
Professor of Medicine

KU LEUVEN

VIB - KU Leuven I Vesalius Research Center – Department of Oncology
Campus Gasthuisberg O&N 4 I Herestraat 49 - B 912, 3000 Leuven I
Phone : +32 16 37 32 35 I Fax : +32 16 37 25 85 I www.vrc-lab.be

Graphical Abstract

Click here to download Graphical Abstract graphical abstr_vierkant 5.5_600.tif

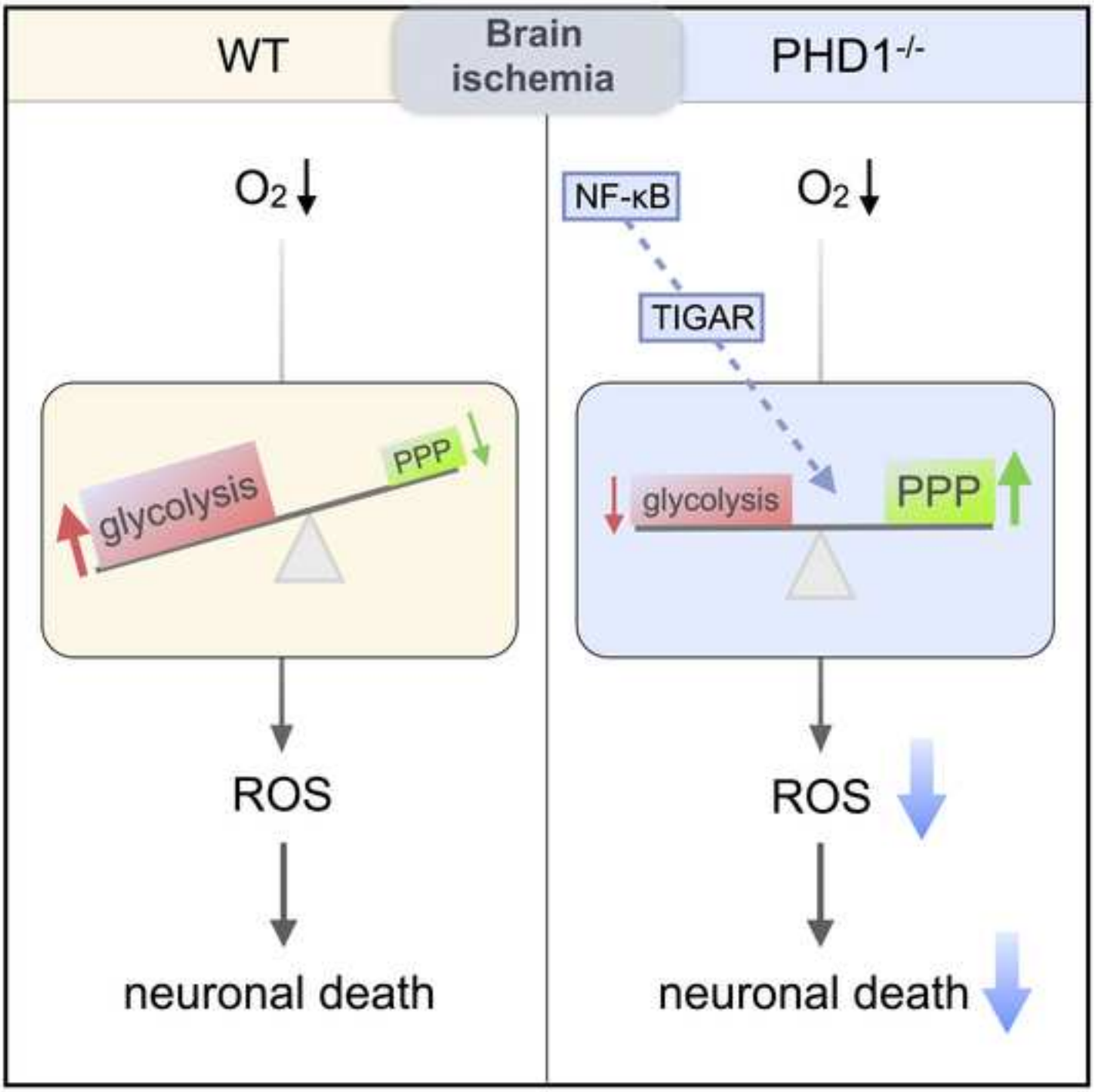

DELETION OR INHIBITION OF THE OXYGEN SENSOR PHD1 PROTECTS AGAINST ISCHEMIC STROKE VIA REPROGRAMMING OF NEURONAL METABOLISM

Annelies Quaegebeur[1,2], Inmaculada Segura[1,2], Roberta Schmieder[3,4], Dries Verdegem[1,2], Ilaria Decimo[1,2], Francesco Bifari[1,2], Tom Dresselaers[5], Guy Eelen[1,2], Debapriva Ghosh[6], Sandra Schoors[1,2], Dorien Broekaert[3,4], Bert Cruys[1,2], Kristof Govaerts[5], Carla De Legher[1,2], Ann Bouché[1,2], Luc Schoonjans[1,2], Matt S. Ramer[1,2,7], Gene Hung[8], Goele Bossaert[9], Don W. Cleveland[10], Uwe Himmelreich[5], Thomas Voets[6], Robin Lemmens[11-13], C. Frank Bennett[8], Wim Robberecht[11-13], Katrien De Bock[1,2], Mieke Dewerchin[1,2], Sarah-Maria Fendt[3,4], Bart Ghesquière[14] & Peter Carmeliet[1,2]*

(1) Laboratory of Angiogenesis and Neurovascular link, Department of Oncology, University of Leuven, Leuven, Belgium; (2) Laboratory of Angiogenesis and Neurovascular link, Vesalius Research Center, VIB, Leuven, Belgium; (3) Laboratory of Cellular Metabolism and Metabolic Regulation, Department of Oncology, University of Leuven, Leuven, Belgium; (4) Laboratory of Cellular Metabolism and Metabolic Regulation, Vesalius Research Center, VIB, Leuven, Belgium; (5) Biomedical MRI/Mosaic, Department of Imaging and Pathology, University of Leuven, Leuven, Belgium; (6) Laboratory of Ion Channel Research and TRP channel research platform Leuven, Department of Cellular and Molecular Medicine, University of Leuven, Leuven, Belgium; (7) International Collaboration on Repair Discoveries, the University of British Columbia, Vancouver, Canada; (8) Isis Pharmaceuticals, Carlsbad, CA; (9) Leuven Statistics Research Centre (LStat), University of Leuven, Leuven, Belgium; (10) Ludwig Institute for Cancer Research, Department of Medicine and Neuroscience, University of California, San Diego, La Jolla, CA 92093, USA; (11) Laboratory of Neurobiology, Vesalius Research Center, VIB, Leuven, Belgium; (12) Experimental Neurology (Department of Neurosciences) and Leuven Research Institute for Neuroscience and Disease (LIND), University of Leuven, Leuven, Belgium; (13) Neurology, University Hospitals Leuven, Leuven, Belgium; (14) Metabolomics Expertise Center, Vesalius Research Center, VIB, Leuven, Belgium.

*: current address: Department Health Sciences and Technology, Laboratory of Exercise and Health, Swiss Federal Institute of Technology (ETH) Zurich, Zurich, Switzerland.

Editorial correspondence: P. Carmeliet, M.D., Ph.D.
Laboratory of Angiogenesis and Neurovascular link
Vesalius Research Center
VIB, KU Leuven, Campus Gasthuisberg O&N4
Herestraat 49 - 912,
B-3000, Leuven, Belgium
tel: 32-16-37.32.02; fax: 32-16-37.25.85
e-mail: peter.carmeliet@vib-kuleuven.be

SUMMARY

The oxygen-sensing prolyl hydroxylase domain proteins (PHDs) regulate cellular metabolism, but their role in neuronal metabolism during stroke is unknown. Here we report that PHD1 deficiency provides neuroprotection in a murine model of permanent brain ischemia. This was not due to an increased collateral vessel network. Instead, PHD1$^{-/-}$ neurons were protected against oxygen-nutrient deprivation by reprogramming glucose metabolism. Indeed, PHD1$^{-/-}$ neurons enhanced glucose flux through the oxidative pentose phosphate pathway by diverting glucose away from glycolysis. As a result, PHD1$^{-/-}$ neurons increased their redox buffering capacity to scavenge oxygen radicals in ischemia. Intracerebroventricular injection of PHD1-antisense oligonucleotides reduced the cerebral infarct size and neurological deficits following stroke. These data identify PHD1 as a regulator of neuronal metabolism and a potential therapeutic target in ischemic stroke.

INTRODUCTION

The brain relies primarily on oxidative glucose metabolism (Mergenthaler et al., 2013). However, it remains poorly understood how neurons adapt their metabolism upon ischemic neuronal injury. There is even debate about the metabolism of neurons in baseline conditions and it remains largely unknown if neuronal metabolism is a target to promote neuroprotection. This is nonetheless an important question, as ischemic stroke is the 4th leading cause of death and a common reason of severe disability. Reperfusion and neuroprotection are two therapeutic strategies aiming to rescue the ischemic penumbra. This region, surrounding a core of necrotic tissue, suffers moderate blood flow reduction, and remains viable during a limited period before a failure of energy and redox homeostasis causes neuronal death. Despite progress in preclinical studies, there are no clinically approved neuroprotective treatments.

Prolyl hydroxylase domain proteins (PHD1-3) are master regulators of the response to hypoxia (Quaegebeur and Carmeliet, 2010; Wong et al., 2013). As their hydroxylation of target proteins is oxygen-dependent, PHDs act as oxygen sensors. The transcription factors hypoxia-inducible factor (HIF)-1α and HIF-2α are PHD targets, yet other targets exist (Wong et al., 2013). When oxygen is present, PHD-mediated hydroxylation targets proteins for proteasomal degradation. Thus, when oxygen levels drop and PHDs lose their activity, HIFs and other target proteins accumulate (Wong et al., 2013).

Little is known about the functions of PHDs in the brain. PHDs instruct metabolic adaptations, but this has been primarily studied in cell types other than neurons. Through stabilization of HIFs, PHD inhibition induces a shift from oxidative to glycolytic metabolism (Aragones et al., 2009). For instance, loss of PHD1 makes the muscle and liver ischemia-tolerant by reducing their mitochondrial respiration (Aragones et al., 2008; Schneider et al., 2009). However, it is unknown if PHDs similarly control neuronal metabolism, and if HIFs are their primary target. Here, we examined the role of PHD1 in brain ischemia and focused on its role in controlling neuronal metabolism.

RESULTS

PHD1$^{-/-}$ MICE ARE PROTECTED AGAINST BRAIN ISCHEMIA

To assess if PHDs regulate brain ischemia, we performed a permanent middle cerebral artery occlusion (pMCAO) in PHD1$^{-/-}$ and PHD3$^{-/-}$ mice, and in neural-specific PHD2 deficient mice (PHD2^{NKO} mice). Staining with vital dye 2,3,5-triphenyltetrazolium chloride (TTC) revealed that the ischemic injury was largely attenuated in PHD1$^{-/-}$ mice (71 % reduction in infarct size; Fig. 1A-C) but not in PHD2^{NKO} and PHD3$^{-/-}$ mice (Fig. 1D-I). PHD1$^{-/-}$ mice on a 129S6 background (Fig. S1A-C) were similarly protected (Fig. 1A-C). Use of the adhesive tape removal test to quantify functional deficits after pMCAO showed that a delay in time to sense and remove the tape on the affected paw was nearly prevented in PHD1$^{-/-}$ mice (Fig. 1J,K). Transcript levels of *Phd2* and *Phd3* were not compensatorily elevated in PHD1$^{-/-}$ brains (mRNA copies/10^3 copies *HPRT*: 13.9 ± 0.4 in WT and 14.7 ± 0.7 in PHD1$^{-/-}$ for *Phd2*; 2.2 ± 0.1 in WT and 2.3 ± 0.1 in PHD1$^{-/-}$ for *Phd3*; n = 4; p = NS).

PHD1 DEFICIENCY DOES NOT CAUSE VASCULAR CHANGES IN THE BRAIN

We investigated a possible vascular mechanism underlying the neuroprotection in PHD1$^{-/-}$ mice, as PHDs regulate vessel growth and perfusion (Quaegebeur and Carmeliet, 2010). Perfusion with FITC-conjugated dextran showed a similar area of perfused vessels in the cortical area of (non-stroked) WT *vs* PHD1$^{-/-}$ brains (Fig. 2A-C). Vascular corrosion casting showed a similar number of pial collaterals in WT and PHD1$^{-/-}$ brains (Fig. 2D-F). Also, staining for α-smooth muscle actin (α-SMA) did not reveal genotypic differences in conducting arterioles (Fig. S2A-C). Circulating erythropoietin and hematocrit levels were also unaltered in PHD1$^{-/-}$ mice (Aragones et al., 2008).

We also assessed if vessel perfusion was improved in PHD1$^{-/-}$ mice upon pMCAO. Calculating the fraction of perfused vessels in the stroke area *vs* contralateral cortex, by identifying vessels with isolectin-B4 staining and perfusion with FITC-dextran injection, did not show a difference in PHD1$^{-/-}$ mice in the stroke area or contralateral side (Fig. 2G-K).

Also, magnetic resonance imaging showed a smaller lesion in PHD1$^{-/-}$ mice at 24 hours after arterial occlusion (Fig. 2L,M), despite a similar perfusion deficit (Fig. 2N). All these data indicate that the neuroprotective effect of PHD1 loss is not due to vascular changes.

PHD1 DEFICIENCY PROTECTS AGAINST OXYGEN-NUTRIENT DEPRIVATION

We then hypothesized that PHD1 deficiency might confer neuroprotection by modulating intrinsic neuronal properties, and therefore exposed 7 days *in vitro* (DIV) cortical neurons to two hours of oxygen-nutrient deprivation after which they were re-exposed to ambient air and nutrient-rich medium (Meloni et al., 2011). After 24 hours, neuronal cell death (measured by LDH release) was reduced in PHD1$^{-/-}$ neurons (Fig. 2O).

Transcript and protein levels of PHD2 and PHD3 were not compensatorily upregulated in PHD1$^{-/-}$ neurons (Fig. S2D-E). Also, PHD2 and PHD3 silencing in WT neurons did not confer protection against oxygen-nutrient deprivation (Fig. 2P), all indicating a PHD1-specific effect. The PHD1$^{-/-}$ neuroprotection was also not attributable to structural differences in PHD1$^{-/-}$ embryos or different PHD1$^{-/-}$ neuronal culture features (Fig. S2F-K). Also, mRNA levels of neurotrophic factors and their receptors were not affected by PHD1 deficiency (Table S1).

PHD1 DEFICIENCY REPROGRAMS CENTRAL CARBON METABOLISM

In muscle, PHD1 deficiency protects against ischemia by lowering mitochondrial respiration and the production of reactive oxygen species (ROS) via a shift to glycolysis (Aragones et al., 2008). Surprisingly, however, glycolysis, glucose consumption and glucose oxidation were reduced in PHD1$^{-/-}$ neurons in baseline conditions (Fig. 3A-C). The change in glucose oxidation was not due to a decrease in the number of mitochondria (mtDNA/gDNA ratio: 1.595 ± 0.065 in WT *vs* 1.565 ± 0.032 in PHD1$^{-/-}$; n = 3; p = NS) or mitochondrial density (TOMM20 staining) (Fig. S3A-E). PHD1 deficiency did also not alter mitochondrial oxygen consumption (Fig. 3D,E; Fig. S3F). As these results (reduced glucose oxidation but similar oxygen consumption in PHD1$^{-/-}$ neurons) were unexpected,

we sought to explain this apparent paradox. We hypothesized that oxidation of alternative substrates might be enhanced. Whereas lactate oxidation was unaffected (pmol lactate/h/10^6 cells: 10,510 ± 3,120 for WT *vs* 10,440 ± 2,660 for PHD1$^{-/-}$; n = 3; p = NS), glutamine oxidation was enhanced in PHD1$^{-/-}$ neurons (Fig. 3F).

These data suggest that the decrease in ATP production due to the reduction of glucose oxidation was compensated, at least in part, by enhanced production of ATP from increased glutamine oxidation. As a result, PHD1 deficiency did not alter the energy charge ([ATP] + ½ [ADP]) / ([ATP] + [ADP] + [AMP]): 0.947 ± 0.005 for WT *vs* 0.942 ± 0.005 for PHD1$^{-/-}$; n = 6; p = NS) or the levels of ATP, ADP and AMP (Fig. S3G). Also, dendritic branching (relying on mitochondrial ATP production (Oruganty-Das et al., 2012)) and other energy-consuming processes (Na^+/K^+ pump activity, RNA and protein synthesis) were not altered in PHD1$^{-/-}$ neurons (Fig. S3H-U), implying that PHD1 deficiency in neurons did not induce general energy hypometabolism. Overall, in contrast to PHD1$^{-/-}$ muscle, PHD1$^{-/-}$ neurons did not show a shift from oxidative to glycolytic metabolism, yet maintained mitochondrial metabolism and energy homeostasis, and lowered their glycolytic flux. Notably, the reduced glycolysis was not due to transcriptional changes in glycolytic genes (Table S2).

PHD1$^{-/-}$ NEURONS ENHANCE THE OXPPP FLUX

Glycolysis in neurons is kept at a low rate to enable flux of glucose into the oxidative pentose phosphate pathway (oxPPP), in which glucose oxidation converts [$NADP^+$] to [NADPH]. The latter is of vital importance as a reducing equivalent to replenish the pool of reduced glutathione (GSH) from oxidized glutathione (GSSG) to maintain redox homeostasis in neurons (Herrero-Mendez et al., 2009). Given this reciprocal regulation of glycolysis and oxPPP, we hypothesized that the reduced glycolysis was part of a glucose rerouting towards the oxPPP. Indeed, PHD1$^{-/-}$ neurons showed a 2.8-fold induction in oxPPP flux levels (Fig. 4A), or when corrected for glycolytic levels (see methods), a 8.7-fold relative increase in oxPPP (n = 4). Thus, in the absence of PHD1, more glucose from glycolysis is redirected towards the oxPPP.

MOLECULAR REGULATION OF THE OXPPP BY PHD1 DEFICIENCY

The increased oxPPP was not due to an increased "passive" shunting of accumulating glycolytic intermediates to the oxPPP (Fig. 3B; Fig. S4A). Also, we did not detect genotypic differences in mRNA levels of glucose-6-phosphate dehydrogenase (G6PD), a rate-limiting enzyme of the oxPPP (Fig. S4B), or in G6PD activity (nmol NADH/min/mg protein: 0.433 ± 0.109 for WT *vs* 0.432 ± 0.109 for PHD1$^{-/-}$; n = 4; p = NS).

TP53-inducible glycolysis and apoptosis regulator (TIGAR) acts as a putative regulator of the glycolysis/oxPPP crossroad by redirecting glucose away from glycolysis into the oxPPP (Bensaad et al., 2006), but its function in neurons is poorly characterized. *TIGAR* transcript levels were 2.2-fold higher in PHD1$^{-/-}$ than WT neurons (Fig. 4B), whereas silencing of PHD2 or PHD3 did not affect *TIGAR* transcript levels (mRNA copies per 10^3 copies *ß-actin*: 0.10 ± 0.01 in ctrl WT, 0.11 ± 0.02 in PHD2^{KD} and 0.11 ± 0.01 in PHD3^{KD} neurons, p = NS). TIGAR also functionally regulated the oxPPP flux, since overexpression of TIGAR in WT neurons increased oxPPP levels (Fig. S4C), while silencing of TIGAR in PHD1$^{-/-}$ neurons reduced the oxPPP flux (Fig. S4D). Thus, PHD1 deficiency increased the oxPPP flux by regulating TIGAR expression.

PHD1 DEFICIENCY IMPROVES THE ROS SCAVENGING CAPACITY

The oxPPP generates NADPH, which is used as a reducing equivalent by glutathione reductase to regenerate reduced glutathione (Stanton, 2012), a major anti-oxidant in neurons (Dringen, 2000). An increased oxPPP flux would imply an improved H_2O_2 scavenging capacity. When measuring ROS levels by CM-H_2DCF labeling upon H_2O_2 administration, PHD1$^{-/-}$ neurons showed a less steep increase in CM-H_2DCF fluorescence intensity (Fig. 4C), implying accelerated H_2O_2 detoxification. Notably, MitoSox levels were not reduced in baseline conditions in PHD1$^{-/-}$ neurons, arguing against a reduced mitochondrial ROS production (Fig. S4E-G). G6PD silencing, which reduced the oxPPP flux in PHD1$^{-/-}$ neurons (Fig. S4H,I), decreased the scavenging capacity more in PHD1$^{-/-}$ than WT neurons (Fig. 4D), suggesting that the improved ROS scavenging capacity of PHD1$^{-/-}$ neurons was dependent, at least in part, on an increased oxPPP flux. Gene

expression analysis of anti-oxidant enzymes did not show enhanced expression upon PHD1 deficiency (Table S3).

PHD1 DEFICIENCY MAINTAINS A RESIDUAL OXPPP FLUX IN HYPOXIA

For the oxPPP to provide redox equivalents for neuroprotection during oxygen deprivation (as during stroke), it should remain operational during hypoxia in PHD1$^{-/-}$ neurons. Like in non-neuronal cell types (Aragones et al., 2009), hypoxia increased the glycolytic flux in neurons, yet glycolysis remained lower in hypoxic PHD1$^{-/-}$ than WT neurons (Fig. 4E). Hypoxia almost nullified the oxPPP flux in WT neurons, while PHD1$^{-/-}$ neurons were still able to maintain a residual oxPPP flux, nearly in the range of normoxic WT neurons (Fig. 4F). Notably, the genotypic differences in glucose and glutamine oxidation were maintained in hypoxia as well (Fig. S4J,K). Thus, by reprogramming glucose metabolism and maintaining a residual oxPPP flux, PHD1 deficiency ensured a low but vital residual level of redox homeostasis, especially during ischemia. Indeed, measurements of oxidized (GSSG) and reduced (GSH) glutathione after 2 hours of oxygen-nutrient deprivation revealed that the glutathione redox state was less oxidized in PHD1$^{-/-}$ neurons (Fig. 4G).

CONFIRMATION OF THE PHD1-DEFICIENT PHENOTYPE

Also in “aged” embryonic cortical neurons, cultured for 21 DIV as a surrogate model of adult neurons (Martin et al., 2008), PHD1 deficiency reduced glycolysis (by 25 ± 0.5 %; n = 4; $p < 0.05$) while increasing oxPPP (by 2.2 ± 0.4 fold; n = 3; $p < 0.05$). In addition, using established methods (Ayala et al., 2006; Buescher et al., 2015), we infused [1,2-^{13}C]-glucose in adult conscious and unrestrained mice and measured in microdissected hippocampi the mass isotopomer distribution in pentose-5-phosphate sugars (pool of ribose-5-P and other pentoses) at the interface between the oxPPP and non-oxPPP, i.e. the non-oxidative branch of the PPP that generates ribose-5-P from glycolytic intermediates, however without production of NADPH. We used the ratio of the M+1 *vs* M+2 labeling of pentose-5-phosphate as a parameter of the importance of the oxPPP vs non-oxPPP (Fig. 5A). The M+1 *vs* M+2 labeling of pentose-5-phosphates was enriched

more in PHD1$^{-/-}$ than WT hippocampi (0.97 ± 0.03 in PHD1$^{-/-}$ *vs* 0.87 ± 0.01 in WT; n = 4-5; p < 0.05). Thus, similar to cultured neurons, the oxPPP was enhanced in the neuron-enriched hippocampus of PHD1$^{-/-}$ mice *in vivo*. Further, PHD1$^{-/-}$ mice showed lower GSSG levels in the ischemic hemisphere, indicating that PHD1 deficiency enables the ischemic brain to improve its redox maintenance (Fig. 5B).

ISCHEMIC PROTECTION IN PHD1$^{-/-}$ NEURONS IS HIF-INDEPENDENT

We investigated if the effects of PHD1 deficiency relied on PHD1's hydroxylase activity. We thus transduced PHD1$^{-/-}$ neurons with a vector expressing wild type PHD1 (PHD1^{WT}) or a hydroxylase-inactive PHD1 mutant (PHD1^{D311A}) (McNeill et al., 2002) (Fig. S5A). Re-expression of PHD1^{WT}, but not PHD1^{D311A}, in PHD1$^{-/-}$ neurons aggravated neuronal death compared to control PHD1$^{-/-}$ neurons after oxygen-nutrient deprivation (Fig. 6A), indicating that inhibition of the hydroxylation activity of PHD1 mediates its neuroprotective effect.

Next, we explored the involvement of HIF-1α or HIF-2α. Immunoblotting showed that HIF-1α protein levels were not elevated in normoxic PHD1$^{-/-}$ neurons or PHD1$^{-/-}$ brain (Fig. 6B,C), while HIF-2α protein was not detectable. Levels of HIF-1α transcriptional targets *Vegfa*, *Enolase* and *Pdk1* were not different either (Fig. S5B). PHD1 deficiency did also not interfere with the hypoxic stabilization of HIF-1α, as evidenced by a similar increase in HIF-1α protein levels and transcriptional targets in hypoxia (Fig. 6B; Fig. S5B). Notably, silencing of HIF-1α or HIF-2α did not affect *TIGAR* transcript levels in PHD1$^{-/-}$ neurons (mRNA copies per 10^3 copies *HPRT*: 12.2 ± 3.0 in ctrl PHD1$^{-/-}$, 13.1 ± 2.8 in HIF-1α^{KD} PHD1$^{-/-}$ and 12.7 ± 3.4 in HIF-2α ^{KD} PHD1$^{-/-}$ neurons, n = 5, p = NS). Also, silencing of HIF-1α, HIF-2α or HIF-1ß (which results in blockade of both HIF-1α and HIF-2α) did not abolish the protection against oxygen-nutrient deprivation by PHD1 deficiency (Fig. 6D,E). All these data suggest a HIF-independent mechanism of the PHD1-mediated protection.

POSSIBLE MOLECULAR MECHANISM OF PHD1 DEFICIENCY

We then sought to provide further insight into the underlying molecular mechanism. Reduced PHD1 activity has been linked to enhanced NF-κB activity in non-neuronal cell types, putatively via reduced hydroxylation and hence reduced degradation of I-κB kinase 2 (IKK2) (Scholz and Taylor, 2013). IKK2 activates the NF-κB pathway by phosphorylation of IκBα, chaperone of the NF-κB transcription factor p65, resulting in degradation of IκBα and hence release of p65. Use of a NF-κB luciferase reporter showed that PHD1 deficiency increased the NF-κB promoter activity (Fig. 6F), while protein levels of p65 were also elevated in PHD1$^{-/-}$ neurons (Fig. 6G, Fig. S5C). Further, silencing of *RelA* (p65) reduced the oxPPP flux and TIGAR levels in PHD1$^{-/-}$ neurons (Fig. 6H,I). These data indicate that NF-κB signaling downstream of PHD1 deficiency acts as metabolic regulator of the oxPPP flux via expression of TIGAR.

ICV DELIVERY OF ANTI-PHD1 OLIGONUCLEOTIDES PROTECTS AGAINST BRAIN ISCHEMIA

To test the translational potential of PHD1 inhibition in the brain, we used antisense oligonucleotides (ASOs). Incubation of cultured neurons with the anti-PHD1 ASO lowered *Phd1* mRNA levels by 84%, without affecting transcript or protein levels of PHD2 or PHD3 (Fig. 7A,B). Intracerebroventricular (ICV) delivery of anti-PHD1 ASO lowered brain *Phd1* mRNA levels (Fig. 7C), reduced infarct size (Fig. 7D-G), and improved the performance in the adhesive tape removal test (Fig. 7H,I).

DISCUSSION

The main findings of our study are that PHD1 is an important regulator of neuronal metabolism, providing protection against ischemic redox imbalance. The lack of a clear vascular phenotype in PHD1$^{-/-}$ brains is compatible with previous reports in the brain and other organs in PHD1$^{-/-}$ mice, in which vascular effects were not observed either (Aragones et al., 2008; Chen et al., 2012; Schneider et al., 2009).

PHD1 ORCHESTRATES NEURONAL GLUCOSE METABOLISM

Neurons rely on oxidative glucose metabolism, but the metabolic adaptations during stroke remained largely enigmatic. We show that PHD1 is a key regulator of glucose metabolism in neurons, and orchestrates a protective response against an ischemic insult. Unexpectedly, at least based on previous results that PHD1 deficiency induces a shift towards glycolysis in other cell types (Aragones et al., 2009; Quaegebeur and Carmeliet, 2010), this ischemia tolerance in PHD1$^{-/-}$ neurons relies on an increase in oxPPP at the expense of glycolysis. This reprogramming of glucose metabolism in baseline conditions prepares neurons better against ischemia by providing a greater capacity to scavenge oxygen radicals.

This mechanism is strikingly different from the mechanism whereby PHD1 controls ischemia tolerance in muscle fibers and hepatocytes (Aragones et al., 2008; Schneider et al., 2009). In these cells, PHD1 deficiency induces a switch from oxidative to glycolytic metabolism as a means of oxygen-independent energy generation and reduction of mitochondrial ROS production. By contrast, PHD1 loss in neurons did not alter oxygen consumption and reduced – not increased – glycolytic flux. Also, the ischemia tolerance in PHD1$^{-/-}$ myocytes and hepatocytes relied on HIF-activation (Aragones et al., 2008; Schneider et al., 2009), while this was not the case in PHD1$^{-/-}$ neurons. Hence, PHD1 has a distinct role in neurons as compared to other cell types, and neurons reprogram their metabolism in a (perhaps even unique) PHD1-dependent manner.

Neurons lacking PHD1 shunted more glucose into the oxPPP. This pathway is critical for redox homeostasis by generating NADPH, necessary to replenish reduced glutathione (Stanton, 2012). In agreement, $PHD1^{-/-}$ neurons had an improved capacity to scavenge oxygen radicals. Given that oxidative stress in brain ischemia can contribute to neuronal death (Chan, 2001; Moskowitz et al., 2010), the increase in oxPPP flux can confer protection. Importantly, PHD1 deficiency did not only promote the oxPPP flux in normoxic but also in hypoxic conditions, and better preserved the redox state of glutathione in ischemic stress. In fact, unlike WT neurons, $PHD1^{-/-}$ neurons still had a residual oxPPP flux during hypoxia. Even though smaller than in normoxia, this residual flux was of vital importance to secure sufficient redox homeostasis during hypoxic stress. These findings identify PHD1 as a regulator of the oxPPP and the associated oxygen radical scavenging capacity.

The role of the PPP in stroke has received little attention. G6PD is the rate-limiting enzyme of the oxPPP, which is upregulated in ischemia (Li et al., 2014), while TIGAR promotes the oxPPP at the expense of glycolysis. In line with our findings, inhibition of the oxPPP flux by silencing G6PD aggravated stroke outcome (Zhao et al., 2012), while TIGAR protects against ischemic brain injury, though oxPPP flux measurements were not performed in these studies (Cao et al., 2015; Li et al., 2014). Some evidence suggests a contextual role of the PPP, attributing opposing fates to NADPH. As a reducing co-factor of glutathione reductase, NADPH improves the anti-oxidant capacity, but as an electron donor of NADPH oxidase, NADPH can also generate superoxides (Stanton, 2012), explaining the divergent effects of PPP manipulation on ischemic neuroprotection (Cao et al., 2015; Herrero-Mendez et al., 2009; Li et al., 2014; Suh et al., 2008; Zhao et al., 2012) Regardless of these additional possible effects, regulation of the oxPPP by PHD1 deficiency resulted in improved – not impaired – anti-oxidant capacity.

MECHANISMS OF OXPPP REGULATION BY PHD1

Our study implies a role of NF-κB signaling downstream of PHD1 in the regulation of the oxPPP flux in neurons. In line with our findings, NF-κB signaling has been reported to

lower glycolysis (Mauro et al., 2011). Our findings also indicate that the neuroprotective effect of PHD1 deficiency relies on the hydroxylation activity of PHD1, but not on HIF-signaling, likely because HIF-1α levels are more importantly controlled by PHD2 than by PHD1 (Appelhoff et al., 2004; Myllyharju, 2013). Another reason why HIF-1α levels were not upregulated in PHD1$^{-/-}$ neurons may relate to the finding that ROS levels were decreased in PHD1$^{-/-}$ neurons. Since ROS inactivate PHDs (Quaegebeur and Carmeliet, 2010), reduced ROS levels are expected to result in less inactivated PHD2 and PHD3, which would favor the degradation of HIF-1α. Hence, this mechanism is expected to counteract any possible upregulation of HIF-1α by loss of PHD1.

ISCHEMIA TOLERANCE IN PHD1$^{-/-}$ BRAIN: DISTINCT FROM HYPOMETABOLISM?

We also considered if basal hypometabolism might explain the ischemia tolerance in PHD1$^{-/-}$ neurons, as various lines of evidence suggest such a link. First, hibernating animals cope with oxygen starvation by depressing oxidative metabolism (often by lowering oxygen consumption by > 50-fold) and by reducing protein synthesis and other energy-consuming processes (Fraisl et al., 2009; Larson et al., 2014). Second, in the mammalian brain, hypoxia signaling has been implicated in inducing hypometabolism and other putatively protective responses, elicited by ischemic preconditioning (Quaegebeur and Carmeliet, 2010), even though a direct contribution to neuroprotection in acute ischemic events remains outstanding.

However, the ischemia tolerance of PHD1$^{-/-}$ neurons is distinct from the aforementioned phenomena. Indeed, loss of PHD1 in neurons is *not* accompanied by a reduction in oxygen consumption or energy conservation (as evidenced by the maintained Na^+/K^+ pump activity, dendritic branching, protein and RNA synthesis). Although we cannot exclude a slight energy hypometabolism in PHD1$^{-/-}$ neurons (below the detection threshold of our techniques), we were not able to pick up genotypic differences when measuring energy consumption and production. Instead, PHD1 deficiency in neurons is characterized by reduced glycolysis and glucose oxidation, but increased oxPPP and glutamine oxidation, and maintained lactate oxidation and oxygen consumption, i.e.

metabolic changes that are opposite to those accompanying hypometabolism during hibernation or ischemic preconditioning. Such a metabolic reprogramming underlying ischemia tolerance has not been reported previously.

TRANSLATIONAL POTENTIAL OF PHD1 INHIBITION

Our data show that hypoxia increases glycolysis, which can deprive neurons from a vitally important PPP flux. Interestingly, in cell culture and animal models of neurodegenerative disorders, signs of increased glycolysis have been sporadically described (D'Alessandro et al., 2011; Ferreira et al., 2011; Rodriguez-Rodriguez et al., 2012; Yao et al., 2009), raising the speculative question whether a similar metabolic shift is taking place in these conditions, and whether PHD1 inhibition would be beneficial as well in these diseases.

Silencing of PHD1 by ICV delivery of antisense oligonucleotides prior to stroke protected against brain ischemia, thus phenocopying the genetic data. However, a clinically more relevant strategy would be to administer a PHD1 inhibitor after stroke onset. Unfortunately, we had no access to a PHD1-selective chemical inhibitor to test how rapidly PHD1 blockade would induce ischemia tolerance. Despite this limitation, our prevention studies raise the question if PHD1 inhibition might be clinically useful to diminish neuronal damage in conditions where the risk of cerebral ischemia is considered high, such as upon a critical carotid stenosis or following a subarachnoid hemorrhage, though possible clinical benefit of such strategy awaits further study.

A therapy based on blocking PHD1 may also differ from existing stroke treatments, relying on blocking oxygen radicals by administering anti-oxidants. Indeed, many of those treatments neglected the importance of physiological signaling by oxygen radicals in neurons, partly explaining the poor translational success (Moskowitz et al., 2010). PHD1 inhibition is a fundamentally different and perhaps more appealing approach, as it relies on switching on an endogenous protective mechanism. Future research will clarify if PHD1 inhibition is valid for neuroprotection when initiated after stroke onset. The development of selective (preferably blood brain barrier-permeable) PHD1 inhibitors will be instrumental in shaping clinical indications for PHD1 inhibition and directing further studies.

EXPERIMENTAL PROCEDURES

Detailed methods are described in the Supplement.

MOUSE STRAINS: PHD1$^{-/-}$ (Aragones et al., 2008), PHD2$^{lox/lox}$ (Mazzone et al., 2009) and PHD3$^{-/-}$ (Aragones et al., 2008) mice were described. PHD2$^{lox/lox}$ mice were intercrossed with Nestin-Cre mice (Tronche et al., 1999) to obtain neural specific PHD2 deficient mice. Housing and experimental animal procedures were approved by the Institutional Animal Care and Research Advisory Committee of the University of Leuven, Belgium.

STROKE MODEL: Brain ischemia was induced using the pMCAO model (Kuraoka et al., 2009). Infarct size was analyzed at 24 hours after ischemia by vital dye staining of 1 mm coronal brain slices (Bederson et al., 1986), and infarction area was calculated as the ratio of the unstained area over the total bihemispheric area, using Image J. Functional impact of the stroke was tested using the adhesive tape removal test (Bouet et al., 2009).

BRAIN VASCULATURE: Arteries were analyzed by immunostaining for αSMA; vessel perfusion after tail vein injection with fluorescein isothiocyanate (FITC)-conjugated dextran; pial collateral circulation via vascular corrosion casting (Krucker et al., 2006) and counting of the number of collaterals per hemisphere. The stroke-induced perfusion deficit in the brain was measured by magnetic resonance imaging at 2 and 24 hours after pMCAO.

NEURONAL CULTURE: Cortical neurons were prepared from cortices of embryonic day 14.5 or 15.5 mice, pooled from one litter (Thathiah et al., 2009). Gene silencing was done after 2 days using gene-specific lentiviral shRNA vectors. Oxygen-nutrient deprivation was initiated after 7 days in culture by exposure for 2 hours to 0.1% oxygen in nutrient-deprived medium followed by re-exposure to ambient air and regular medium.

METABOLIC FLUX ASSAYS: Glycolysis, oxPPP, glucose, glutamine and lactate oxidation

were measured using radiolabeled tracers. Glucose consumption was defined as the difference in glucose concentration in medium after 24 hours and was measured via liquid chromatography-mass spectrometry (LC-MS). OCR was measured using the extracellular flux analyzer XF24 (SeaHorse Bioscience). ROS scavenging was measured using CM-H_2-DCFDA. GSSG/GSH levels were determined using LC-MS. ATP/ADP/AMP levels were determined using HPLC. Intracellular Na^+ concentration was monitored using SBFI-based microfluorimetry.

IMMUNOCYTOCHEMISTRY was done on cortical neurons grown for 7 days on Willco-Dish glass bottom dishes (Ibidi), using the antibodies listed in the Supplement.

RNA, DNA AND PROTEIN ANALYSIS: Gene expression was analyzed by quantitative RT-PCR, using premade primer sets (Applied Biosystems). The amount of mitochondrial DNA relative to nuclear genomic DNA was determined by quantitative PCR using primers for cytochrome b (mitochondrial) and RPL13A (nuclear). Immunoblotting was done using the antibodies listed in the Supplement with signal detection using the ECL system (Amersham Biosciences, GE Healthcare).

ICV DELIVERY OF OLIGONUCLEOTIDES: ASOs against murine PHD1 mRNA were designed by Isis Pharmaceuticals. Mice were treated with ASOs by ICV infusion for 10 days using Alzet® osmotic pumps (Cupertino) connected with a catheter to a brain infusion cannula. Two weeks after the infusion, pMCAO was performed.

STATISTICS: All data are mean ± SEM of the indicated number of experiments or mice, unless otherwise noted (median). For the *in vitro* data, the “n” values indicate the number of independent experiments performed with different cultures of WT and PHD1$^{-/-}$ cortical neurons (independent isolations). For the *in vivo* experiments, two-sided Student’s t-tests were used and done using Prism v5.0, considering $p < 0.05$ statistically significant. In some PHD1$^{-/-}$ mice, no infarct was visible after ligation of the middle cerebral artery

(indicating complete protection against ischemia). In these cases, we used non-parametrical Mann-Whitney-U test to determine statistical differences. For *in vivo* experiments, investigators were blinded for treatment or genotype. For *in vitro* experiments, statistical significance between groups was calculated on n pooled independent experiments using linear mixed-effect model statistics to correct for effects by inter-experimental variation (Schoors et al., 2015). Calculations were done using R and the lme4 package. In all cases, the condition was entered as fixed effect. P-values were obtained with the Kenward-Roger F-test for small mixed effect model datasets using lmerTest package. Again, $p < 0.05$ was considered statistically significant. For the time course experiments with CM-H_2DCF fluorescence, we used linear mixed-effect model statistics to determine the slope and statistical differences between slopes.

ACKNOWLEDGEMENTS

Funding support: Research Foundation–Flanders (FWO) (AQ, IS, BG, KDB, SMF); FP7 Marie Curie Intra-European Fellowship (ID, FB); Pegasus Marie Curie-FWO (RQ); senior clinical investigator of FWO Flanders (RL); Agency for Innovation by Science and Technology in Flanders (IWT) (BC, SS). The work of PC is supported by a Federal Government Belgium grant (IUAP P7/03), long-term structural Methusalem funding by the Flemish Government, grants from the FWO (G.0671.12N, 1.5.244.11N) and Foundation Leducq Transatlantic Network (ARTEMIS), funding by “A cure for ALS” from ALS Liga Belgium, Motor Neuron Disease Association, ALS Association (ID#C44128), the European Research Council und the European’s Seventh Framework Programme (FP7/2007-2013)/ ERC grant agreement n° 340429, European Community's Health Seventh Framework Programme (FP7/2007-2013) under grant agreement n° 259867.

AUTHORSHIP CONTRIBUTIONS

PC conceptualized and AQ conducted the project. AQ, IS, RS, ID, FB, TD, GE, DG, DB, KG, AB, CDL, MSR performed experiments. AQ, IS, RS, DV ID, FB, TD, GE, DG, MSR, UH, TV, RL, SMF and BG designed experiments and analyzed data. DWC, CFB and GH provided the ASO design and advice on ASO-experiments. IS, ID, FB, SS, GE, GB, LS, RL, KDB, WR, MD, SMF and BG provided scientific suggestions and contributed to the manuscript review. AQ and PC wrote the manuscript. All authors edited the paper.

CONFLICT-OF-INTEREST DISCLOSURE

G. Hung and C.F. Bennett are employees of Isis Pharmaceuticals Inc. and could benefit if a therapeutic product for treatment of ischemic stroke results from this work.

REFERENCES

Appelhoff, R. J., Tian, Y. M., Raval, R. R., Turley, H., Harris, A. L., Pugh, C. W., Ratcliffe, P. J., and Gleadle, J. M. (2004). Differential function of the prolyl hydroxylases PHD1, PHD2, and PHD3 in the regulation of hypoxia-inducible factor. J Biol Chem *279*, 38458-38465.

Aragones, J., Fraisl, P., Baes, M., and Carmeliet, P. (2009). Oxygen sensors at the crossroad of metabolism. Cell Metab *9*, 11-22.

Aragones, J., Schneider, M., Van Geyte, K., Fraisl, P., Dresselaers, T., Mazzone, M., Dirkx, R., Zacchigna, S., Lemieux, H., Jeoung, N. H.*, et al.* (2008). Deficiency or inhibition of oxygen sensor Phd1 induces hypoxia tolerance by reprogramming basal metabolism. Nat Genet *40*, 170-180.

Ayala, J. E., Bracy, D. P., McGuinness, O. P., and Wasserman, D. H. (2006). Considerations in the design of hyperinsulinemic-euglycemic clamps in the conscious mouse. Diabetes *55*, 390-397.

Bederson, J. B., Pitts, L. H., Germano, S. M., Nishimura, M. C., Davis, R. L., and Bartkowski, H. M. (1986). Evaluation of 2,3,5-triphenyltetrazolium chloride as a stain for detection and quantification of experimental cerebral infarction in rats. Stroke *17*, 1304-1308.

Bensaad, K., Tsuruta, A., Selak, M. A., Vidal, M. N., Nakano, K., Bartrons, R., Gottlieb, E., and Vousden, K. H. (2006). TIGAR, a p53-inducible regulator of glycolysis and apoptosis. Cell *126*, 107-120.

Bouet, V., Boulouard, M., Toutain, J., Divoux, D., Bernaudin, M., Schumann-Bard, P., and Freret, T. (2009). The adhesive removal test: a sensitive method to assess sensorimotor deficits in mice. Nat Protoc *4*, 1560-1564.

Buescher, J. M., Antoniewicz, M. R., Boros, L. G., Burgess, S. C., Brunengraber, H., Clish, C. B., DeBerardinis, R. J., Feron, O., Frezza, C., Ghesquiere, B.*, et al.* (2015). A roadmap for interpreting (13)C metabolite labeling patterns from cells. Curr Opin Biotechnol *34*, 189-201.

Cao, L., Chen, J., Li, M., Qin, Y. Y., Sun, M., Sheng, R., Han, F., Wang, G., and Qin, Z. H. (2015). Endogenous level of TIGAR in brain is associated with vulnerability of neurons to ischemic injury. Neurosci Bull.

Chan, P. H. (2001). Reactive oxygen radicals in signaling and damage in the ischemic brain. J Cereb Blood Flow Metab *21*, 2-14.

Chen, R. L., Nagel, S., Papadakis, M., Bishop, T., Pollard, P., Ratcliffe, P. J., Pugh, C. W., and Buchan, A. M. (2012). Roles of individual prolyl-4-hydroxylase isoforms in the first 24 hours following transient focal cerebral ischaemia: insights from genetically modified mice. J Physiol *590*, 4079-4091.

D'Alessandro, G., Calcagno, E., Tartari, S., Rizzardini, M., Invernizzi, R. W., and Cantoni, L. (2011). Glutamate and glutathione interplay in a motor neuronal model of amyotrophic lateral sclerosis reveals altered energy metabolism. Neurobiol Dis *43*, 346-355.

Dringen, R. (2000). Metabolism and functions of glutathione in brain. Prog Neurobiol *62*, 649-671.

Ferreira, I. L., Cunha-Oliveira, T., Nascimento, M. V., Ribeiro, M., Proenca, M. T., Januario, C., Oliveira, C. R., and Rego, A. C. (2011). Bioenergetic dysfunction in Huntington's disease human cybrids. Exp Neurol *231*, 127-134.

Fraisl, P., Aragones, J., and Carmeliet, P. (2009). Inhibition of oxygen sensors as a therapeutic strategy for ischaemic and inflammatory disease. Nat Rev Drug Discov.

Herrero-Mendez, A., Almeida, A., Fernandez, E., Maestre, C., Moncada, S., and Bolanos, J. P. (2009). The bioenergetic and antioxidant status of neurons is controlled by continuous degradation of a key glycolytic enzyme by APC/C-Cdh1. Nat Cell Biol *11*, 747-752.

Krucker, T., Lang, A., and Meyer, E. P. (2006). New polyurethane-based material for vascular corrosion casting with improved physical and imaging characteristics. Microsc Res Tech *69*, 138-147.

Kuraoka, M., Furuta, T., Matsuwaki, T., Omatsu, T., Ishii, Y., Kyuwa, S., and Yoshikawa, Y. (2009). Direct experimental occlusion of the distal middle cerebral artery induces high reproducibility of brain ischemia in mice. Exp Anim *58*, 19-29.

Larson, J., Drew, K. L., Folkow, L. P., Milton, S. L., and Park, T. J. (2014). No oxygen? No problem! Intrinsic brain tolerance to hypoxia in vertebrates. J Exp Biol *217*, 1024-1039.

Li, M., Sun, M., Cao, L., Gu, J. H., Ge, J., Chen, J., Han, R., Qin, Y. Y., Zhou, Z. P., Ding, Y., and Qin, Z. H. (2014). A TIGAR-regulated metabolic pathway is critical for protection of brain ischemia. J Neurosci *34*, 7458-7471.

Martin, M. G., Perga, S., Trovo, L., Rasola, A., Holm, P., Rantamaki, T., Harkany, T., Castren, E., Chiara, F., and Dotti, C. G. (2008). Cholesterol loss enhances TrkB signaling in hippocampal neurons aging in vitro. Mol Biol Cell *19*, 2101-2112.

Mauro, C., Leow, S. C., Anso, E., Rocha, S., Thotakura, A. K., Tornatore, L., Moretti, M., De Smaele, E., Beg, A. A., Tergaonkar, V.*, et al.* (2011). NF-kappaB controls energy homeostasis and metabolic adaptation by upregulating mitochondrial respiration. Nat Cell Biol *13*, 1272-1279.

Mazzone, M., Dettori, D., Leite de Oliveira, R., Loges, S., Schmidt, T., Jonckx, B., Tian, Y. M., Lanahan, A. A., Pollard, P., Ruiz de Almodovar, C.*, et al.* (2009). Heterozygous deficiency of PHD2 restores tumor oxygenation and inhibits metastasis via endothelial normalization. Cell *136*, 839-851.

McNeill, L. A., Hewitson, K. S., Gleadle, J. M., Horsfall, L. E., Oldham, N. J., Maxwell, P. H., Pugh, C. W., Ratcliffe, P. J., and Schofield, C. J. (2002). The use of dioxygen by HIF prolyl hydroxylase (PHD1). Bioorg Med Chem Lett *12*, 1547-1550.

Meloni, B. P., Meade, A. J., Kitikomolsuk, D., and Knuckey, N. W. (2011). Characterisation of neuronal cell death in acute and delayed in vitro ischemia (oxygen-glucose deprivation) models. J Neurosci Methods *195*, 67-74.

Mergenthaler, P., Lindauer, U., Dienel, G. A., and Meisel, A. (2013). Sugar for the brain: the role of glucose in physiological and pathological brain function. Trends Neurosci *36*, 587-597.

Moskowitz, M. A., Lo, E. H., and Iadecola, C. (2010). The science of stroke: mechanisms in search of treatments. Neuron *67*, 181-198.

Myllyharju, J. (2013). Prolyl 4-hydroxylases, master regulators of the hypoxia response. Acta Physiol (Oxf) *208*, 148-165.

Oruganty-Das, A., Ng, T., Udagawa, T., Goh, E. L., and Richter, J. D. (2012). Translational control of mitochondrial energy production mediates neuron morphogenesis. Cell Metab *16*, 789-800.

Quaegebeur, A., and Carmeliet, P. (2010). Oxygen sensing: a common crossroad in cancer and neurodegeneration. Curr Top Microbiol Immunol *345*, 71-103.

Rodriguez-Rodriguez, P., Fernandez, E., Almeida, A., and Bolanos, J. P. (2012). Excitotoxic stimulus stabilizes PFKFB3 causing pentose-phosphate pathway to glycolysis switch and neurodegeneration. Cell Death Differ *19*, 1582-1589.

Schneider, M., van Geyte, K., Fraisl, P., Kiss, J., Aragones, J., Mazzone, M., Mairbaurl, H., Debock, K., Ho Jeoung, N., Mollenhauer, M.*, et al.* (2009). Loss or silencing of the PHD1 prolyl hydroxylase protects livers of mice against ischemia/referpusion injury. Gastroenterology.

Scholz, C. C., and Taylor, C. T. (2013). Hydroxylase-dependent regulation of the NF-kappaB pathway. Biol Chem *394*, 479-493.

Schoors, S., Bruning, U., Missiaen, R., Queiroz, K. C., Borgers, G., Elia, I., Zecchin, A., Cantelmo, A. R., Christen, S., Goveia, J.*, et al.* (2015). Fatty acid carbon is essential for dNTP synthesis in endothelial cells. Nature *520*, 192-197.

Stanton, R. C. (2012). Glucose-6-phosphate dehydrogenase, NADPH, and cell survival. IUBMB Life *64*, 362-369.

Suh, S. W., Shin, B. S., Ma, H., Van Hoecke, M., Brennan, A. M., Yenari, M. A., and Swanson, R. A. (2008). Glucose and NADPH oxidase drive neuronal superoxide formation in stroke. Ann Neurol *64*, 654-663.

Thathiah, A., Spittaels, K., Hoffmann, M., Staes, M., Cohen, A., Horre, K., Vanbrabant, M., Coun, F., Baekelandt, V., Delacourte, A.*, et al.* (2009). The orphan G protein-coupled receptor 3 modulates amyloid-beta peptide generation in neurons. Science *323*, 946-951.

Tronche, F., Kellendonk, C., Kretz, O., Gass, P., Anlag, K., Orban, P. C., Bock, R., Klein, R., and Schutz, G. (1999). Disruption of the glucocorticoid receptor gene in the nervous system results in reduced anxiety. Nat Genet *23*, 99-103.

Wong, B. W., Kuchnio, A., Bruning, U., and Carmeliet, P. (2013). Emerging novel functions of the oxygen-sensing prolyl hydroxylase domain enzymes. Trends Biochem Sci *38*, 3-11.

Yao, J., Irwin, R. W., Zhao, L., Nilsen, J., Hamilton, R. T., and Brinton, R. D. (2009). Mitochondrial bioenergetic deficit precedes Alzheimer's pathology in female mouse model of Alzheimer's disease. Proc Natl Acad Sci U S A *106*, 14670-14675.

Zhao, G., Zhao, Y., Wang, X., and Xu, Y. (2012). Knockdown of glucose-6-phosphate dehydrogenase (G6PD) following cerebral ischemic reperfusion: the pros and cons. Neurochem Int *61*, 146-155.

FIGURE LEGENDS

FIGURE 1: PHD1 DEFICIENCY PROTECTS AGAINST BRAIN ISCHEMIA

A,B, TTC stained brain slices showing unstained infarct zone (white) from WT (A) and PHD1$^{-/-}$ mice (B) 24 hours after pMCAO. **C,** Quantification of the stroke area (% of total bihemispheric area) (n = 6, Mann-Whitney U test; difference in medians: -5.29 *vs* WT, 95% CI: -6.14 to -0.96). **D-I**, TTC stained brain slices from ctrl (D) *vs* PHD2^{NKO} (E) and from WT (G) *vs* PHD3$^{-/-}$ mice (H). Quantification of the stroke area (% of total bihemispheric area) for ctrl *vs* PHD2^{NKO} mice (n = 3, p = NS; difference in means: +0.21 *vs* ctrl, 95% CI: -2.95 to 3.38) (F), and for WT *vs* PHD3$^{-/-}$ mice (n = 7-8, p = NS; difference in means: +1.41 *vs* WT, 95% CI: -0.51 to 3.32) (I). **J,K,** Measurements of the adhesive tape removal test at 1 day pre- and at day 1, 4, 8 and 11 post-stroke. Average time WT and PHD1$^{-/-}$ mice need to sense the tape on the affected paw (J) (n = 7-8, repeated-measure ANOVA). Average time mice need to remove the tape (K) (n = 7-8, repeated-measure ANOVA). All quantitative data are mean ± SEM. * p < 0.05. See also Figure S1.

FIGURE 2: PHD1 DEFICIENCY DOES NOT ALTER THE BRAIN VASCULATURE

A,B, Representative images of WT (A) and PHD1$^{-/-}$ (B) cortex after FITC-dextran injection. **C,** Quantification of FITC-dextran-positive area as % of cortical area (reflecting vessel perfusion in cortex) (n = 6-7, difference in means: +0.60 *vs* WT, 95% CI: -0.33 to 1.54). **D-E',** Representative images of three-dimensional corrosion casting showing perfused pial vessels in WT (D) and PHD1$^{-/-}$ brain hemisphere (E). D' and E': larger magnification of boxed areas in D and E. Collaterals were counted per hemisphere (arrowheads). **F,** Quantification of pial collaterals per hemisphere in WT *vs* PHD1$^{-/-}$ brains (n = 3-4; difference in means: +0.58 *vs* WT, 95% CI: -2.11 to 3.28). **G-J,** Representative images of FITC-dextran (green) and isolectin (red) staining of stroke area (G,H) and corresponding contralateral cortex area (I,J) of WT (G,I) and PHD1$^{-/-}$ brain (H,J). **K,** Quantification of FITC^{+} (perfused) vessels, as % of total number of isolectin^{+} vessels in the stroke area and contralateral cortex area in WT *vs* PHD1$^{-/-}$ brains (n = 3-5, difference in means: 6.13 *vs*

WT, 95% CI: -8.52 to 20.79 for stroke side, difference in means: -4.6 *vs* WT, 95% CI: -15.3 to 6.1 for contralateral side,). **L**, Representative brain T2 parametric maps from *in vivo* MRI of WT and PHD1$^{-/-}$ mice 24 hours after pMCAO. **M**, Stroke lesion size (µl), as derived from manual delineation on multi-slice T2-weighted MRI images (n = 4-5, difference in means: -4.74 *vs* WT, 95% CI: -9.24 to -0.24). **N**, Area of the ipsilateral hemisphere with perfusion deficit at 2 and 24 hours after pMCAO (n = 4-5; difference in means: +15.28 *vs* WT, 95% CI: -9.58 to 40.13 after 2 hours; and +12.88 *vs* WT, 95% CI: -27.40 to 53.15 after 24 hours). **O,** Neuronal cell death (% of maximal LDH release) over 24 hours after oxygen-nutrient deprivation in WT and PHD1$^{-/-}$ neurons (n = 3). **P**, Neuronal cell death (% of maximal LDH release) over 24 hours after oxygen-nutrient deprivation in PHD2^{KD} and PHD3^{KD} cells (n = 3, p = NS). All quantitative data are mean ± SEM. Bars: 200 µm (A,B,G-J), 1 mm (D,E). * $p < 0.05$. See also Figure S2 and Table S1.

FIGURE 3: PHD1 DEFICIENCY ALTERS NEURONAL METABOLISM

A, Glycolytic flux in WT and PHD1$^{-/-}$ neurons (n = 8). **B,** Glucose consumption in WT and PHD1$^{-/-}$ neurons (n = 3). **C,** Glucose oxidation in WT and PHD1$^{-/-}$ neurons (n = 7). **D,** Mitochondrial OCR_{BAS} in WT and PHD1$^{-/-}$ neurons (n = 5). **E**, Relative change of OCR_{MAX} and OCR_{ATP} compared to OCR_{BAS} (dotted line) in WT and PHD1$^{-/-}$ neurons (n = 3). **F**, Glutamine oxidation in WT and PHD1$^{-/-}$ neurons (n = 8). All quantitative data are mean ± SEM. * $p < 0.05$. See also Figure S3 and Table S2.

FIGURE 4: ENHANCED OXPPP FLUX IN PHD1$^{-/-}$ NEURONS IMPROVES REDOX BALANCE

A, oxPPP flux in WT and PHD1$^{-/-}$ neurons (n = 4). **B,** TIGAR mRNA levels (mRNA copies/10^3 copies HPRT) in WT and PHD1$^{-/-}$ neurons (n = 11). **C,** Left: Increase in CM-H_2DCF fluorescence (% of the fluorescence value in WT neurons at 45 min) after administration of H_2O_2 to WT or PHD1$^{-/-}$ neurons. Right: Slope values of the curves shown left (the lower the slope, the larger the ROS scavenging capacity) (n = 3). For reasons of clarity, only the average of the individual fluorescence values is shown without SEM, since

the statistics were done using the slopes, calculated by linear mixed-effects model statistics on the individual fluorescence values (also in panel D). **D,** Left: Increase in CM-H_2DCF fluorescence (% of the fluorescence value in control (scr) WT neurons at 45 min) over time after administration of H_2O_2 to WT or PHD1$^{-/-}$ neurons with and without G6PD silencing (G6PD^{KD}). Right: Slope values of the curves shown on the left, obtained by linear mixed-effect model statistics on individual fluorescence values (n = 3). The percentage increase in slope value induced by G6PD^{KD} in PHD1$^{-/-}$ neurons (blue *vs* red bar; 40%) is higher than in WT neurons (grey *vs* black bar; 24%). **E,** Glycolytic flux in WT and PHD1$^{-/-}$ neurons in normoxia and hypoxia (0.1% O_2 for 2 hours) (n = 4). **F,** Oxidative PPP flux in WT and PHD1$^{-/-}$ neurons in normoxia and hypoxia (n = 3). **G,** GSSG levels, as % of total glutathione (GSSG + GSH) levels during reperfusion in WT and PHD1$^{-/-}$ neurons (n = 3). All quantitative data are mean ± SEM. * $p < 0.05$. See also Figure S4 and Table S3.

FIGURE 5: OXPPP AND REDOX HOMEOSTASIS DURING ISCHEMIC STRESS *IN VIVO*

A, Scheme depicting glycolysis and the oxidative and non-oxidative branch of the PPP, and the isotopomer distribution of 1,2-^{13}C-glucose in the PPP. M+1 pentose-5-phosphate (P5P) can arise when glucose-6-phosphate (G6P) is converted via the oxidative PPP, while M+2 P5P can arise from the non-oxidative PPP when there is either a net or exchange flux towards P5P. F6P, fructose-6-phosphate; GAP, glyceraldehyd-3-phosphate; PPP, pentose phosphate pathway (for analysis of M+4 P5P, see methods). **B,** Levels of GSSG as % of total glutathione levels in brain hemispheres of WT and PHD1$^{-/-}$ mice after ischemic stroke (n = 5-7; * $p < 0.05$; difference in means: -0.104 *vs* WT, 95% CI: -0.204 to -0.0045). All quantitative data are mean ± SEM.

FIGURE 6: HYDROXYLATION-DEPENDENT, HIF-INDEPENDENT NEUROPROTECTION IN PHD1$^{-/-}$ NEURONS VIA NF-κB REGULATED INCREASE OF OXPPP

A, Neuronal cell death (% of maximal LDH release) in control WT neurons, control PHD1$^{-/-}$ neurons, PHD1$^{-/-}$ neurons expressing WT PHD1 (PHD1^{WT}), and PHD1$^{-/-}$ neurons expressing hydroxylation-inactive PHD1 mutant (PHD1^{D311A}) (n = 5). **B,** Representative

immunoblot showing protein levels of HIF-1α in normoxic and hypoxic WT and PHD1$^{-/-}$ neurons. Densitometric quantification of independent experiments (% of α-tubulin loading control): 41.2 ± 20.1% in WT and 41.9 ± 20.9% in PHD1$^{-/-}$ in normoxia, 129.7± 46.7% in WT and 122.9 ± 46.7% in PHD1$^{-/-}$ in hypoxia, n = 3, p = NS). **C,** Representative immunoblot showing protein levels of HIF-1α in WT and PHD1$^{-/-}$ brains. Densitometric quantification (% of lamin A/C): 58.3 ± 15.4% in WT and 57.7 ± 20.4% in PHD1$^{-/-}$, n = 4, p = NS). **D,** Neuronal cell death (% of maximal LDH release) over 24 hours after oxygen-nutrient deprivation in WT and PHD1$^{-/-}$ neurons upon silencing of HIF-1α (HIF1α^{KD}) or HIF-2α (HIF2α^{KD}) (n = 3). **E,** Neuronal cell death (% of maximal LDH release) over 24 hours after oxygen-nutrient deprivation in WT and PHD1$^{-/-}$ neurons upon silencing of HIF-1ß (n = 3). **F**, NF-κB luciferase reporter activity in WT and PHD1$^{-/-}$ neurons (a.u. arbitrary units, n = 3). **G**, Representative immunoblots of nuclear p65 levels in WT and PHD1$^{-/-}$ neurons. Densitometric quantification of independent experiments (% of loading control β-actin): 113 ± 35% in WT and 190 ± 36% in PHD1$^{-/-}$ neurons, n = 4, p < 0.05). **H**, oxPPP flux in PHD1$^{-/-}$ neurons upon silencing of RelA (RelAα^{KD}) (n = 4). **I,** TIGAR mRNA expression in PHD1$^{-/-}$ neurons upon silencing of RelA (RelAα^{KD}) (n = 8). All quantitative data are mean ± SEM. * p < 0.05. See also Figure S5.

FIGURE 7: ICV DELIVERY OF ANTI-PHD1 ASOS PROTECTS AGAINST BRAIN ISCHEMIA

A, mRNA expression levels of *Phd1, Phd2* and *Phd3* in neuronal cultures, incubated with anti-PHD1 (PHD1-ASO) and control oligonucleotides (ctrl-ASO) (n = 3). **B,** Representative immunoblots showing protein levels of PHD2 and PHD3 in ctrl-ASO and PHD1-ASO treated WT neurons. Densitometric quantification (% of loading control β-actin): 72 ± 17% in ctrl-ASO treated WT neurons and 64 ± 17% in PHD1-ASO treated WT neurons for PHD2, 28 ± 15% in ctrl-ASO treated WT neurons and 28 ± 13% in PHD1-ASO treated WT neurons for PHD3 (n = 3, p = NS). **C**, mRNA expression levels of *Phd1* in brains from control treated and anti-PHD1 ASO treated mice (n = 4-5). **D-F** Representative brain slices after TTC staining, delineating the infarct zone as an unstained area (white), from control mice receiving saline (D), an ASO against human huntingtin (E) or an PHD1-ASO (F), 24

hours after pMCAO. **G,** Quantification of the stroke area (% of total bihemispheric area) (n = 5-11; difference in means: -2.49, 95% CI: -3.76 to -1.22 for PHD1-ASO *vs* saline; and difference in means: -2.66, 95% CI: -4.40 to -0.92 for PHD1-ASO *vs* ctrl-ASO). **H,I,** Measurements of the adhesive tape removal test at 1 day before and at day 1, 4, 7 and 11 post-stroke. Average time mice need to sense the presence of the tape (H) (n = 7-9, p = 0.057, repeated-measure ANOVA). Average time mice need to remove the tape (I) (n = 9 for ctrl-ASO treated mice, n= 7 for PHD1-ASO mice, $p < 0.05$, repeated-measure ANOVA). * $p < 0.05$. All quantitative data are mean ± SEM.

Figure

Click here to download Figure Figure1_031215.tif

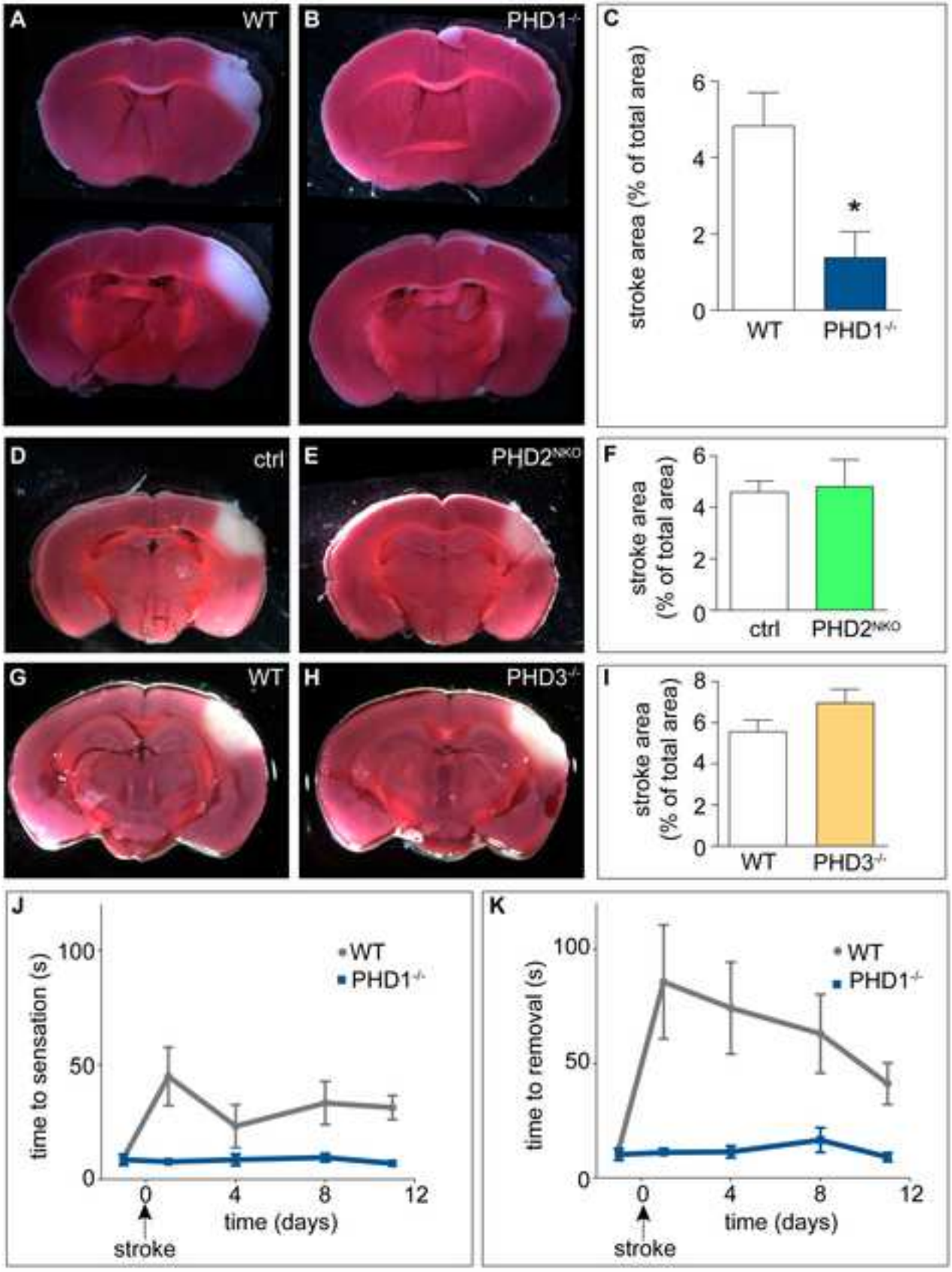

Figure 1

Figure

Click here to download Figure Figure2_031215.tif

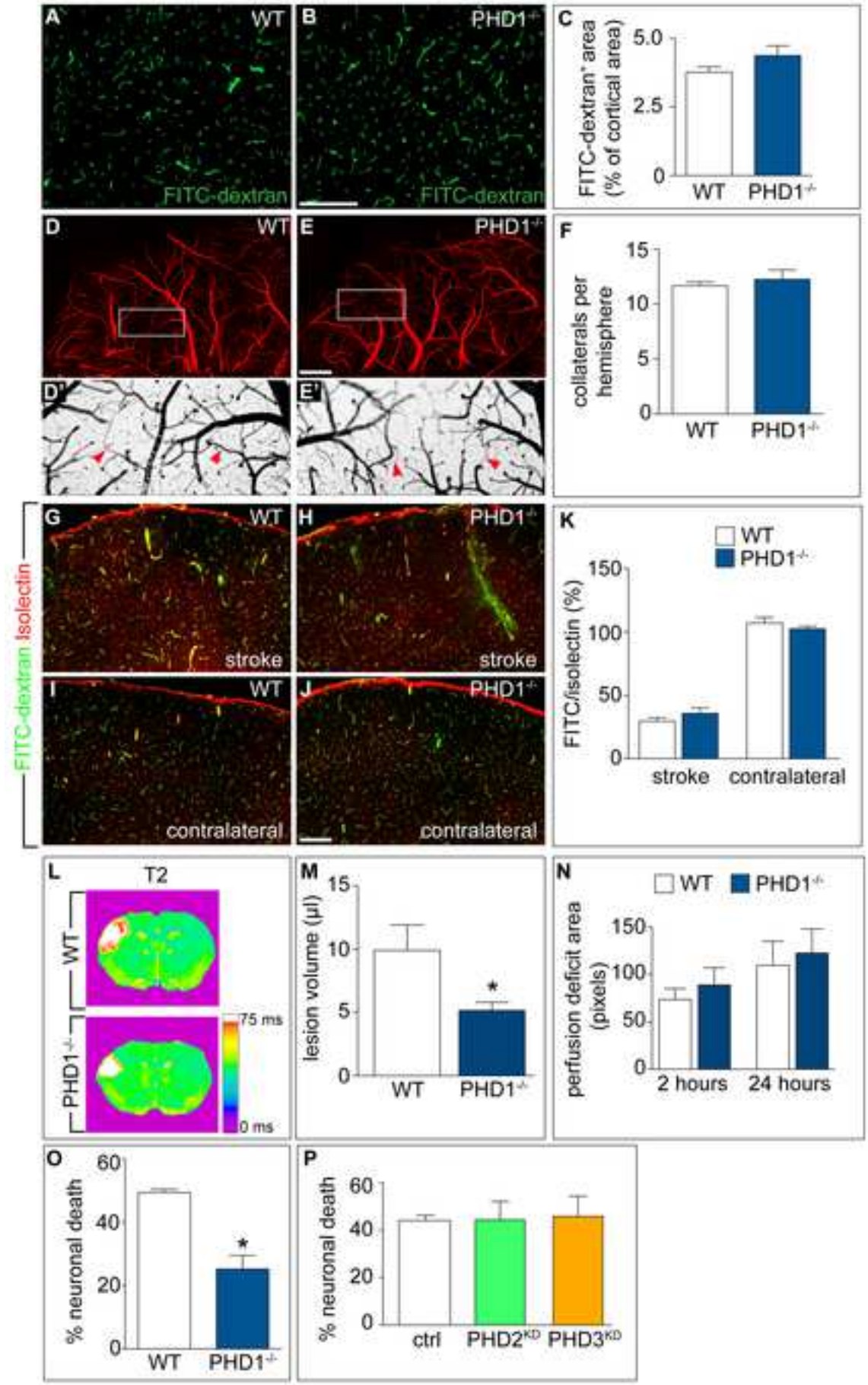

Figure 2

Figure

Click here to download Figure Figure3_031215.tif

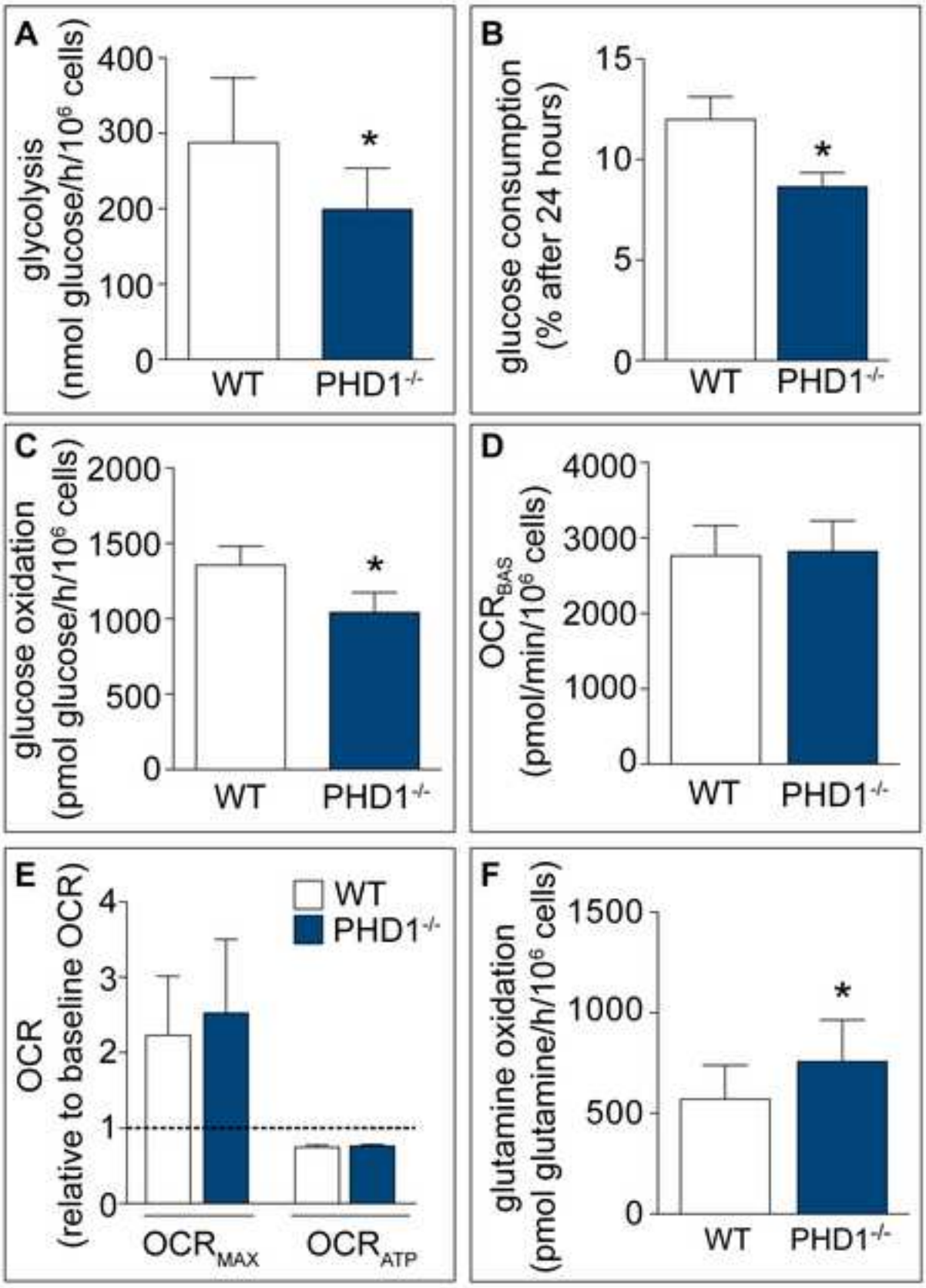

Figure 3

Figure

Click here to download Figure Figure4_031215.tif

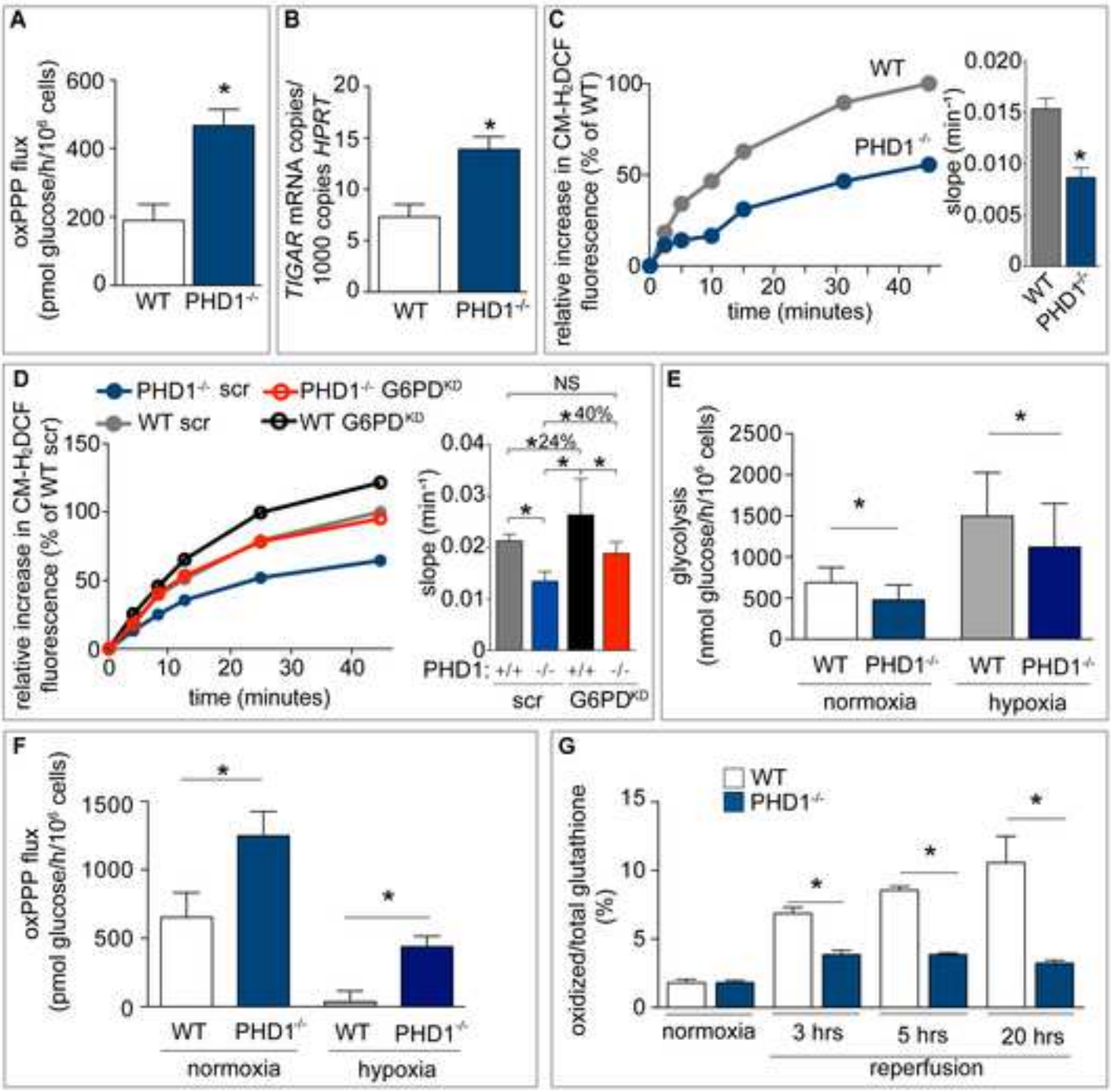

Figure 4

Figure

Click here to download Figure Figure5_031215.tif

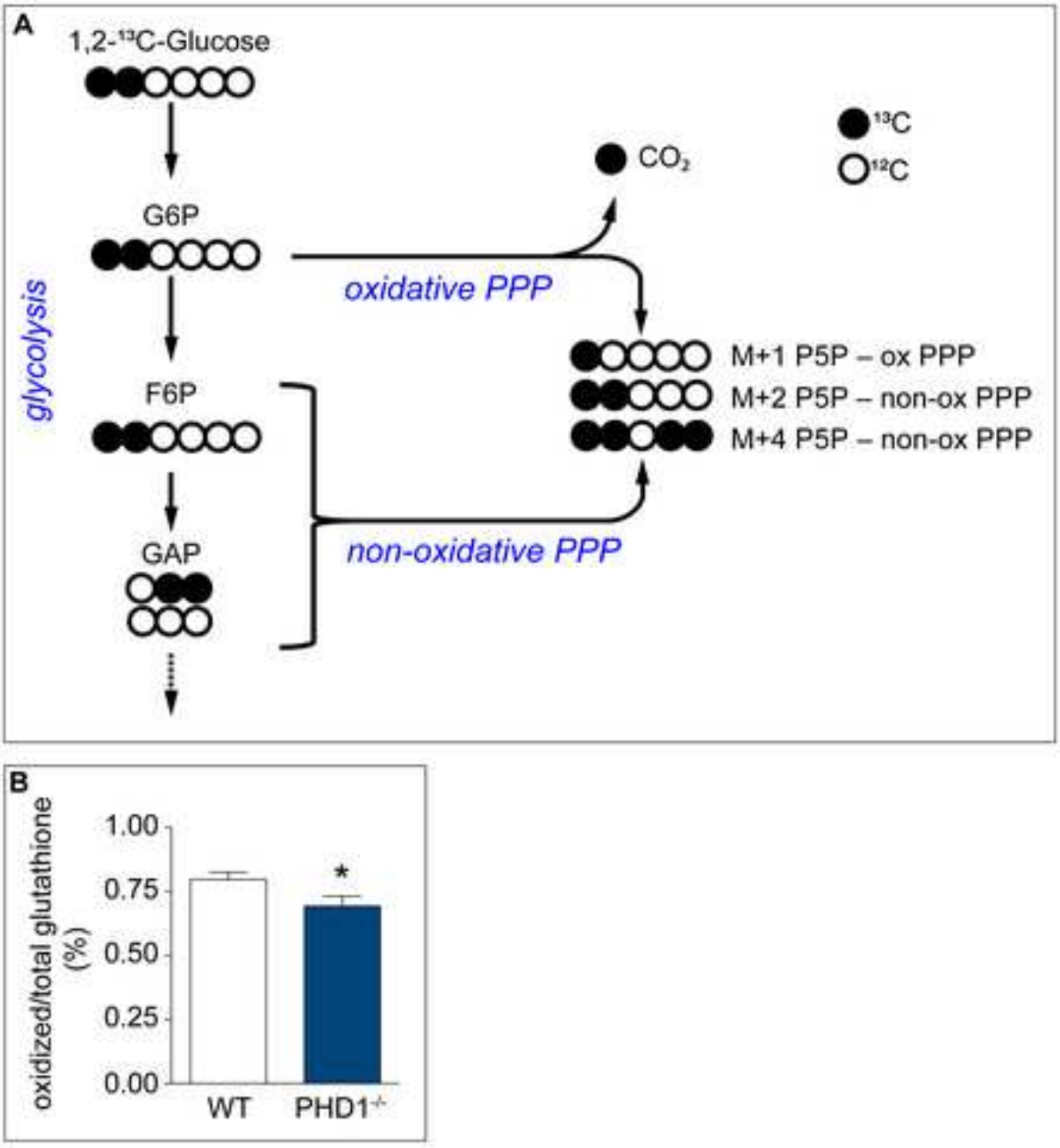

Figure 5

Figure

Click here to download Figure Figure6_031215.tif

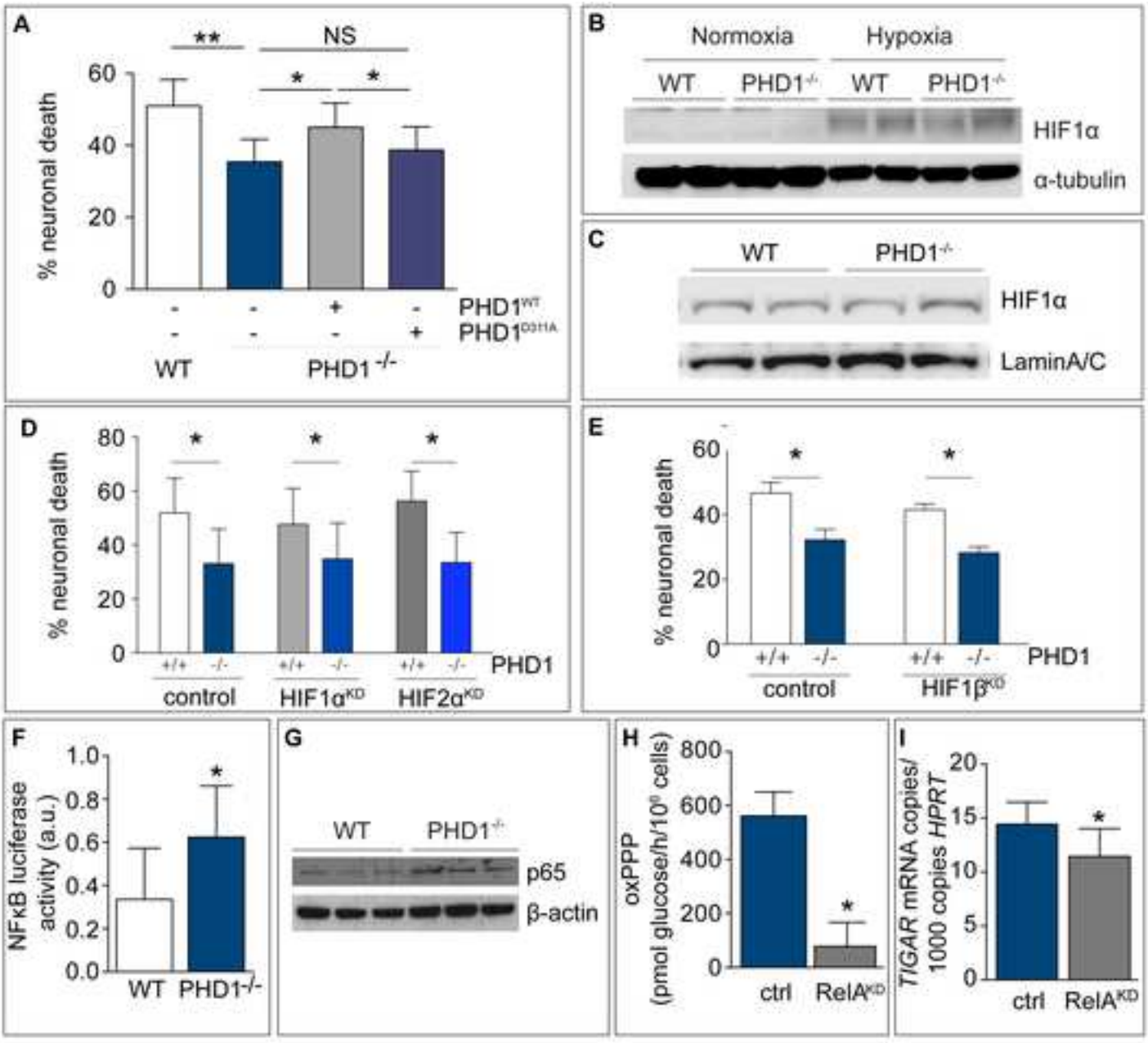

Figure 6

Figure

Click here to download Figure Figure7_031215.tif

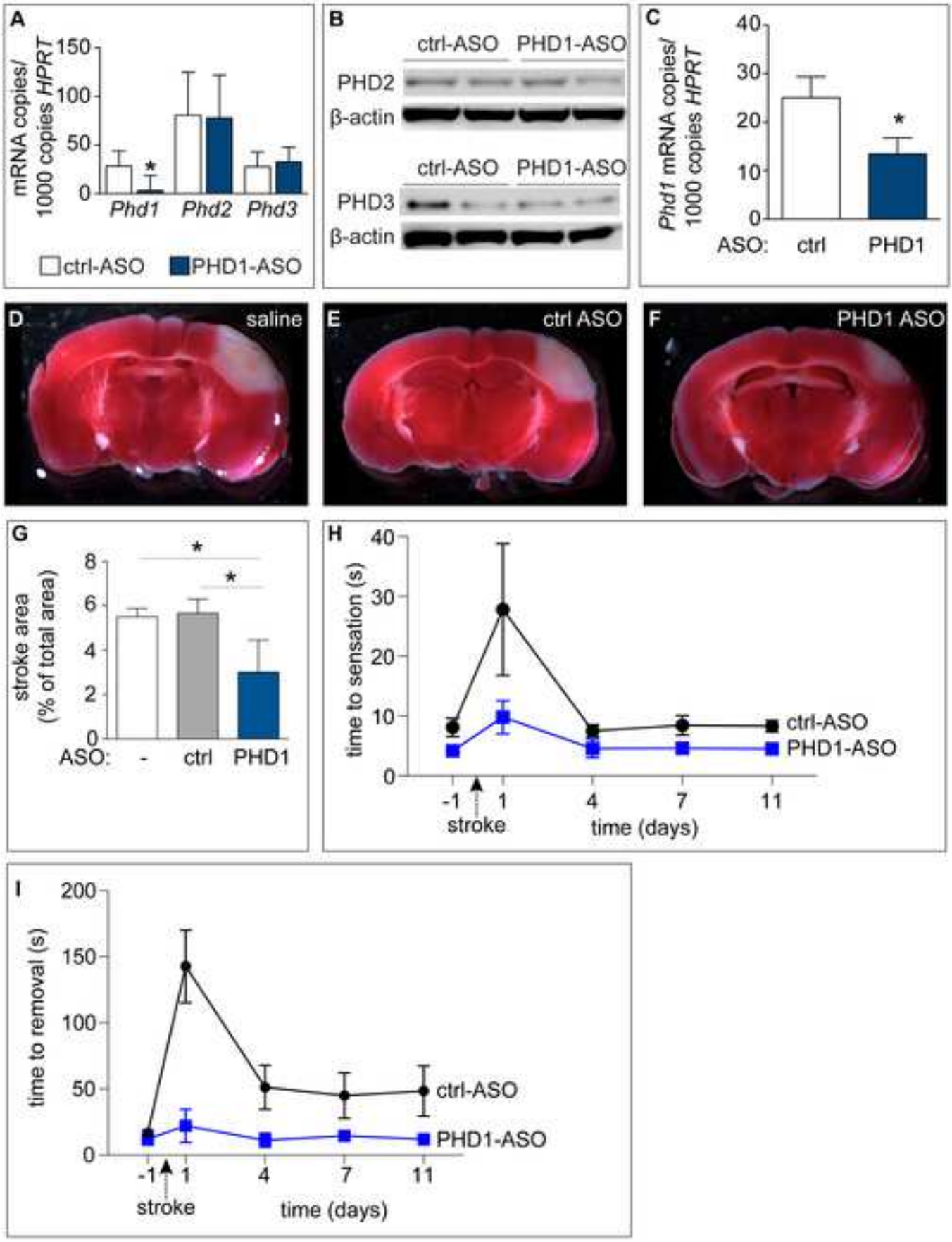

Figure 7

SUPPLEMENTAL INFORMATION

SUPPLEMENTAL DATA

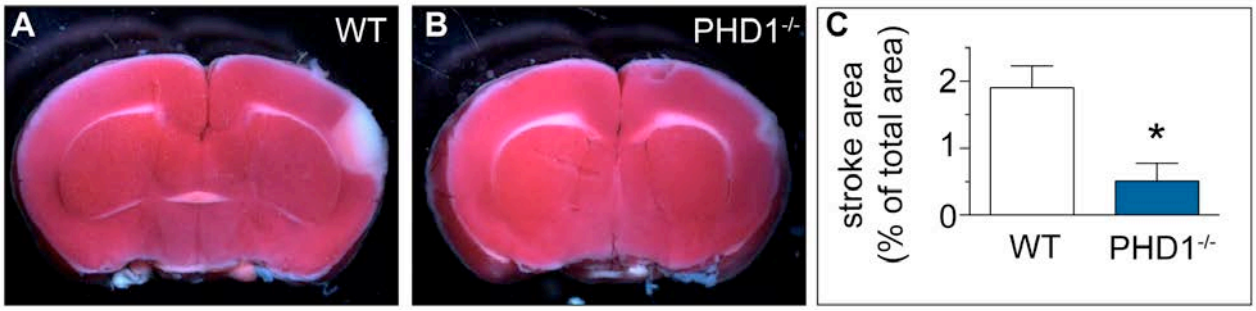

FIGURE S1: RELATED TO FIGURE 1

A,B, TTC stained brain slices showing unstained infarct zone (white) from WT (A) and PHD1$^{-/-}$ mice (B) on a 129S6 background, 24 hours after pMCAO. **C,** Quantification of the stroke area (% of total bihemispheric area) (n = 9 for WT, n = 6 for PHD1$^{-/-}$, * $p < 0.05$ by Mann-Whitney U test; difference in medians: -1.34 *vs* WT, CI 95%: -2.64 to -0.43). Quantitative data are mean ± SEM.

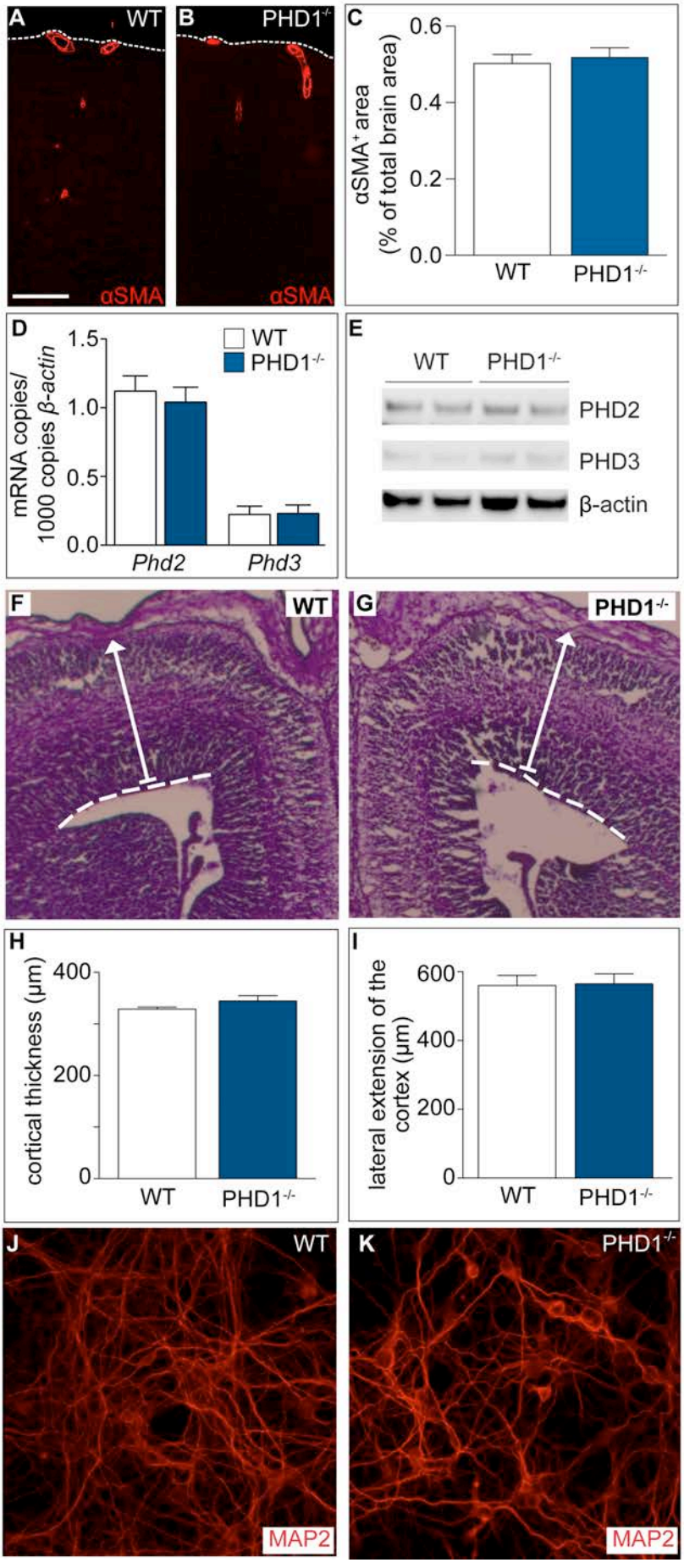
A
WT
αSMA
B
PHD1-/-
αSMA
C
αSMA+ area
(% of total brain area)
0.6
0.4
0.2
0.0
WT
PHD1-/-
D
mRNA copies/
1000 copies β-actin
1.5
1.0
0.5
0.0
WT
PHD1-/-
Phd2
Phd3
E
WT
PHD1-/-
PHD2
PHD3
β-actin
F
WT
G
PHD1-/-
H
cortical thickness (μm)
400
200
0
WT
PHD1-/-
I
lateral extension of the
cortex (μm)
600
400
200
0
WT
PHD1-/-
J
WT
MAP2
K
PHD1-/-
MAP2

FIGURE S2: RELATED TO FIGURE 2

A,B, Representative images of α-SMA immunostained brain sections, visualizing arterioles in WT (A) and PHD1$^{-/-}$ brains (B). **C,** Quantification of α-SMA positive area as percentage of total brain area (n = 4 for WT, n = 5 for PHD1$^{-/-}$, p = NS; difference in means: +0.016 *vs* WT, CI 95%: -0.067 to 0.098). **D,** mRNA expression levels of *Phd2* and *Phd3* in isolated WT and PHD1$^{-/-}$ neurons (n = 3, p = NS). **E,** Representative immunoblots of PHD2 and PHD3 protein levels in WT and PHD1$^{-/-}$ neurons. Densitometric quantification of independent experiments (% of β-actin loading control): 71 ± 36% in WT and 63 ± 36 in PHD1$^{-/-}$ neurons for PHD2, 39 ± 23% in WT and 38 ± 23 in PHD1$^{-/-}$ neurons for PHD3, n = 4, p = NS). **F,G,** Representative Nissl stained coronal brain sections of E14.5 WT (F) and PHD1$^{-/-}$ (G) embryos. The PHD1$^{-/-}$ embryonic brain is comparable to the WT embryonic brain in appearance, cortical thickness (arrow) and lateral extension of the cortex (dashed line), indicative of a normal brain cytoarchitecture. **H,I,** Quantifications of the cortical thickness (H) and lateral extension of the cortex (I) in E14.5 WT and PHD1$^{-/-}$ embryos (n = 3, p = NS; difference in means: +15.6 *vs* WT, 95% CI: -14.9 to 46.1 for cortical thickness (H); and difference in means: +5.23 *vs* WT, 95% CI: -110 to 121 for lateral extension (I)). **J,K,** Representative MAP2 immunostaining of WT (J) and PHD1$^{-/-}$ (K) neuronal cultures showing normal morphological appearance. All quantitative data are mean ± SEM.

TABLE S1: GENE EXPRESSION ANALYSIS OF NEUROTROPHIC FACTORS (RELATED TO FIGURE 2)

GENE	WT NEURONS	PHD1$^{-/-}$ NEURONS
Bdnf	0.0179 ± 0.0109	0.0186 ± 0.0097
Ngf	0.0222 ± 0.0064	0.0228 ± 0.0033
Nt3	0.1306 ± 0.0145	0.1096 ± 0.0084
p75	0.0994 ± 0.0185	0.0966 ± 0.0229
TrkB	2.5642 ± 0.300	2.5292 ± 0.3001
TrkC	1.6391 ± 0.1821	1.6912 ± 0.2192
Vegf-a	1.0260 ± 0.4785	1.1091 ± 0.3366
Vegf-b	1.6121 ± 0.3207	1.6121 ± 0.4357
Vegfr2	0.4526 ± 0.4017	0.2252 ± 0.1330

Quantitative RT-PCR analysis of the mRNA levels of different neurotrophic factors and their receptors in cultured WT and PHD1$^{-/-}$ neurons. Values represent number of mRNA copies/10^3 copies of ß-actin (mean ± SEM, n = 3-6, p = NS). *Bdnf:* Brain-derived neurotrophic factor; *Ngf*: Nerve growth factor; *Nt3*: Neurotrophin 3; *p75*: p75 neurotrophin receptor; *TrkB* and *TrkC*: tyrosine receptor kinase B and C; *Vegf-a* and *Vegf-b*: vascular endothelial growth factor A and B; *Vegfr2*: Vascular endothelial growth factor receptor 2.

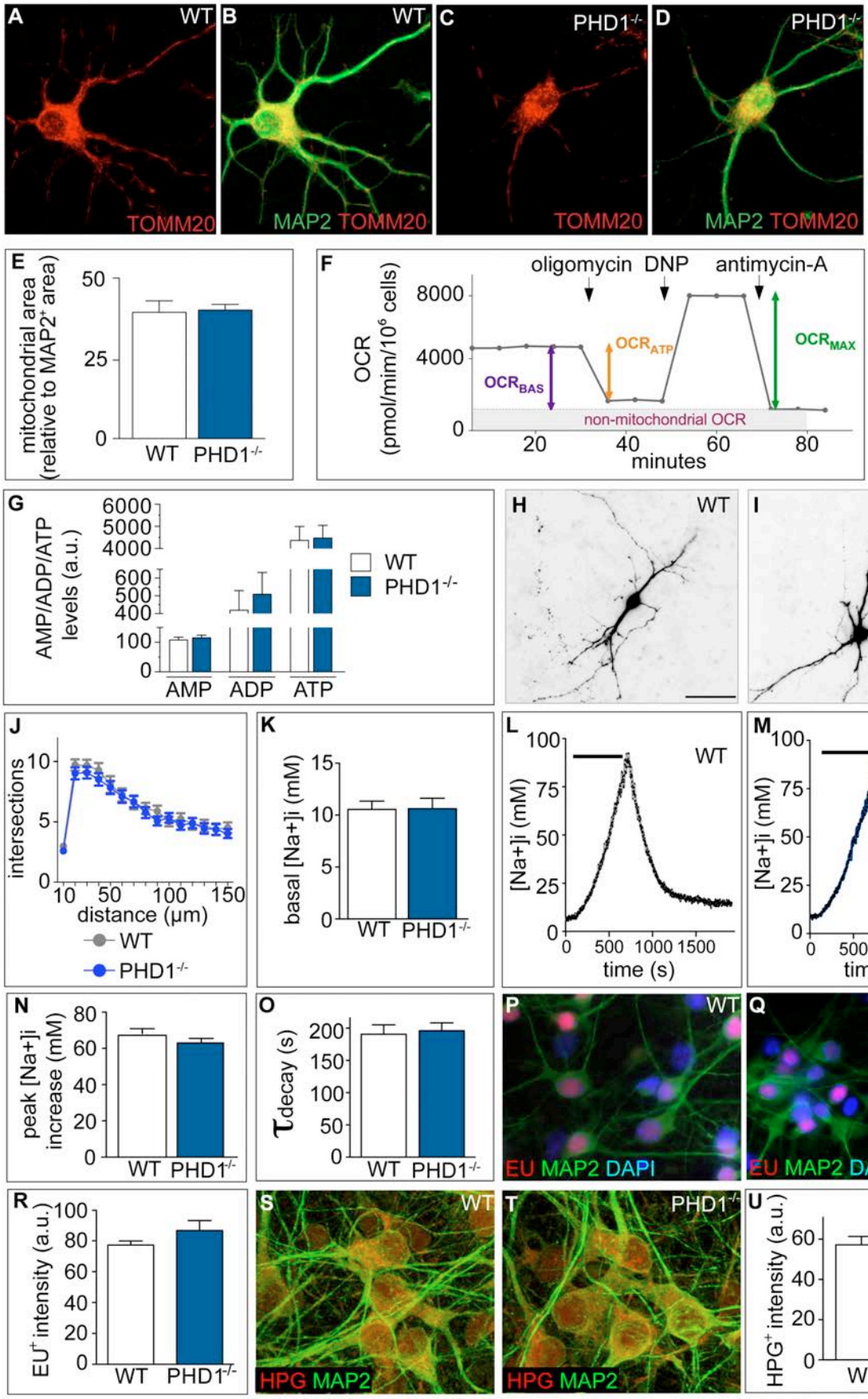
A
WT
TOMM20
B
WT
MAP2 TOMM20
C
PHD1-/-
TOMM20
D
PHD1-/-
MAP2 TOMM20
E
mitochondrial area (relative to MAP2+ area)
50
25
0
WT
PHD1-/-
F
oligomycin
DNP
antimycin-A
OCR (pmol/mim/10^6 cells)
8000
4000
0
OCRBAS
OCRATP
OCRMAX
non-mitochondrial OCR
20
40
60
80
minutes
G
AMP/ADP/ATP levels (a.u.)
6000
5000
4000
600
500
400
100
0
AMP
ADP
ATP
WT
PHD1-/-
H
WT
I
PHD1-/-
J
intersections
10
5
0
10
50
100
150
distance (μm)
WT
PHD1-/-
K
basal [Na+]i (mM)
15
10
5
0
WT
PHD1-/-
L
WT
[Na+]i (mM)
100
75
50
25
0
0
500
1000
1500
time (s)
M
PHD1-/-
[Na+]i (mM)
100
75
50
25
0
0
500
1000
1500
time (s)
N
peak [Na+]i increase (mM)
80
60
40
20
0
WT
PHD1-/-
O
τdecay (s)
200
150
100
50
0
WT
PHD1-/-
P
WT
EU MAP2 DAPI
Q
PHD1-/-
EU MAP2 DAPI
R
EU+ intensity (a.u.)
100
80
60
40
20
0
WT
PHD1-/-
S
WT
HPG MAP2
T
PHD1-/-
HPG MAP2
U
HPG+ intensity (a.u.)
60
40
20
0
WT
PHD1-/-

FIGURE S3: RELATED TO FIGURE 3

A-D, Representative images of neuronal cultures, double-immunostained for TOMM20 (red; A-D) and MAP2 (green; B,D), visualizing the mitochondria and dendritic arbors, respectively, in WT (A,B) and PHD1$^{-/-}$ neuronal cultures (C,D); panels B,D represent the merged image. **E,** Quantification of mitochondrial area (i.e. TOMM20 positive area) per cell (i.e. MAP2 positive area) (n = 3, p = NS). **F,** The Seahorse extracellular flux analyzer allows the measurement of different bioenergetics parameters by sequential injection of different inhibitors of the mitochondrial electron transport chain. Antimycin-A injection allows the calculation of non-mitochondrial OCR and the baseline mitochondrial respiration (OCR_{BAS}). Oligomycin injection allows measuring of respiration coupled to ATP synthesis (OCR_{ATP}) and maximal respiration (OCR_{MAX}) is induced by the uncoupler 2,4-dinitrophenol (DNP). **G,** Levels of AMP, ADP and ATP in WT and PHD1$^{-/-}$ neurons (a.u.: arbitrary units, n = 3; p = NS). **H,I,** Representative images of tandem tomato (tdT)-transfected WT (H) and PHD1$^{-/-}$ (I) neurons after 7 days in culture (shown in gray scale)**. J,** Sholl analysis quantifying neuronal arborization (a process relying on mitochondrial ATP production), expressed as the number of intersections with an overlay of concentric circles positioned at the indicated distances from the soma (n = 52 neurons per genotype; p = NS). **K-O,** Similar activity of the ATP-consuming Na^+/K^+ pump (a main consumer of energy in neurons) in WT and PHD1$^{-/-}$ neurons, indicating that PHD1 deficiency did not induce energy hypometabolism. Intracellular sodium levels in WT and PHD1$^{-/-}$ neurons in baseline (K), and time curves of intracellular sodium concentration ($[Na^+]_i$) as measured by SBFI-fluorescence in WT (L) and PHD1$^{-/-}$ (M) neurons, showing the reversible rise in $[Na^+]_i$ when exposing the cells for 10 minutes to a K^+-free buffer (horizontal bar) instead of the standard K^+-containing buffer; quantifications show the amplitude of the peak of the increase in $[Na^+]_i$ (N) and the time constant of the decay (τ_{decay}) obtained by fitting a monoexponential function to the $[Na^+]_i$ decay phase following readdition of extracellular K^+ (O) (n = 3; p = NS). **P-U,** Panels P-U show experimental evidence of maintained RNA and protein synthesis, indicating that PHD1 deficiency did not induce energy hypometabolism. **P-R,** Representative images of ethinyl uridine (EU, red) staining reflecting similar RNA synthesis in WT (P) and PHD1$^{-/-}$ (Q) neurons, quantified in panel R as EU^+ intensity per

nucleus (DAPI stained, blue) (n = 3; p = NS). Merged images with MAP2 immunostaining (green) and DAPI staining are shown. **S-U,** Representative images of L-homopropargylglycine (HPG, red) staining showing similar protein synthesis in WT (S) and PHD1$^{-/-}$ (T) neurons (MAP2^{+} staining, green), quantified in (U) as HPG^{+} intensity per MAP2^{+} area (n = 2 ; p = NS). A.u., arbitrary units.

TABLE 2: GENE EXPRESSION ANALYSIS OF GLYCOLYTIC ENZYMES (RELATED TO FIGURE 3)

GENE	WT NEURONS	PHD1$^{-/-}$ NEURONS
Glut-1	11.03 ± 4.53	8.52 ± 3.36
Glut-3	35.96 ± 6.20	35.54 ± 6.22
Hk1	178.50 ± 12.32	206.22± 16.89
Pfk1	65.36 ± 4.29	63.45 ± 4.87
Pfkfb3	15.79 ± 14.42	14.44 ± 13.51
Gapdh	69.09 ± 45.13	69.86 ± 47.13
Pgam2	19.29 ± 4.56	22.10 ± 5.91
Eno	49.05 ± 12.27	49.05 ± 12.27
Ldh-a	441.20 ± 53.94	509.05 ± 28.29
Pdk1	79.44 ± 46.60	87.92 ± 57.45

Quantitative RT-PCR data of the mRNA levels of different glycolytic genes in WT and PHD1$^{-/-}$ neurons in baseline conditions. Values represent number of mRNA copies/10^3 copies of HPRT (mean ± SEM, n = 3-4, p = NS). *Glut*: glucose transporter; *Hk1*: hexokinase; *Pfk*: phosphofructokinase; *Pfkfb*: 6-phosphofructo-2-kinase/fructose-2,6-biphosphatase; *Gapdh*: glyceraldehyde-3-phosphate dehydrogenase; *Eno:* Enolase; *Pgam2*: phosphoglycerate mutase 2; *Ldh-a*: lactate dehydrogenase a; *Pdk1*: pyruvate dehydrogenase kinase, isoform 1.

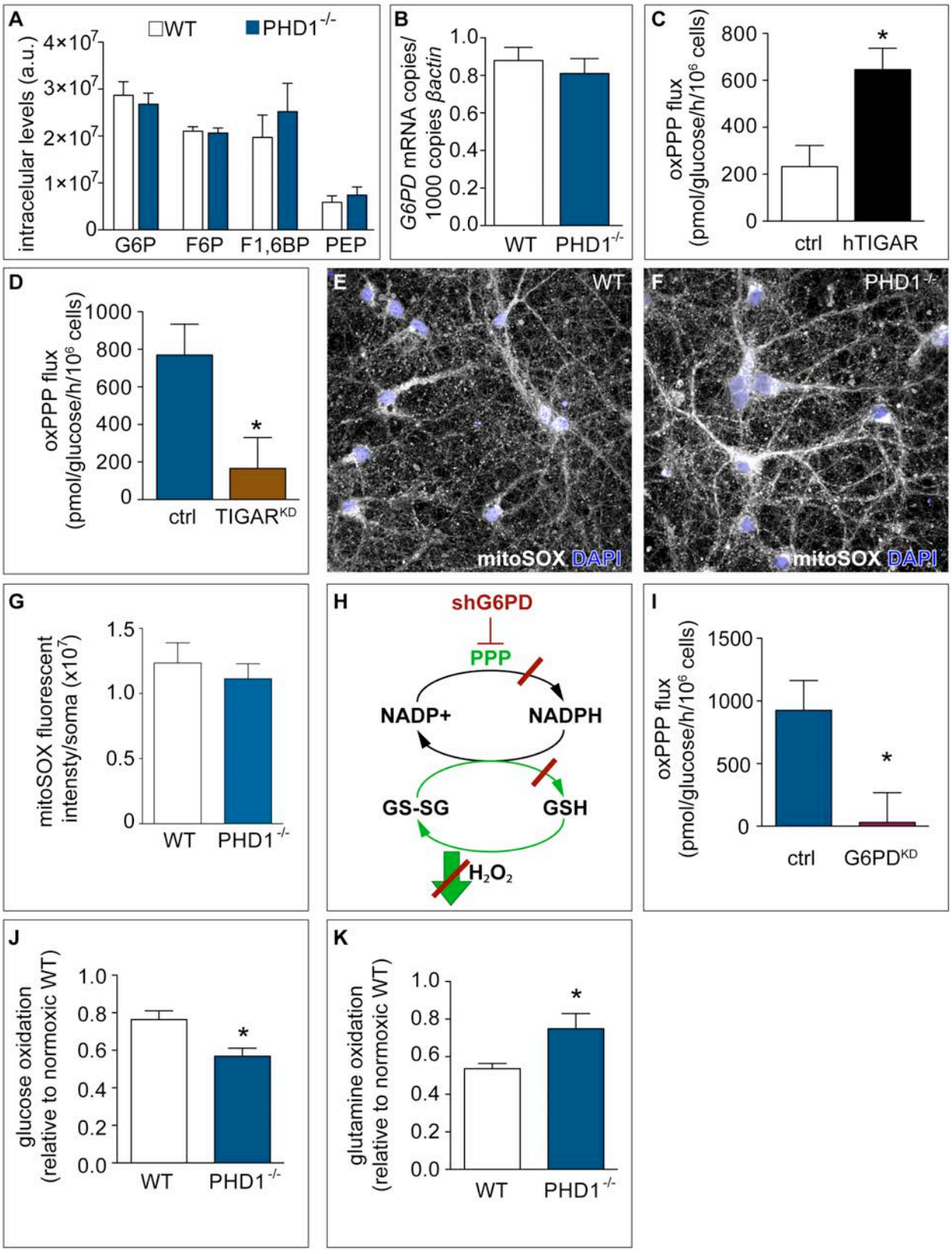
A
WT
PHD1-/-
intracelular levels (a.u.)
4×10^7
3×10^7
2×10^7
1×10^7
0
G6P
F6P
F1,6BP
PEP
B
G6PD mRNA copies/
1000 copies βactin
1.0
0.8
0.6
0.4
0.2
0.0
WT
PHD1-/-
C
oxPPP flux
(pmol/glucose/h/10^6 cells)
800
600
400
200
0
*
ctrl
hTIGAR
D
oxPPP flux
(pmol/glucose/h/10^6 cells)
1000
800
600
400
200
0
*
ctrl
TIGARKD
E
WT
mitoSOX DAPI
F
PHD1-/-
mitoSOX DAPI
G
mitoSOX fluorescent
intensty/soma (x10^7)
1.5
1.0
0.5
0
WT
PHD1-/-
H
shG6PD
PPP
NADP+
NADPH
GS-SG
GSH
H2O2
I
oxPPP flux
(pmol/glucose/h/10^6 cells)
1500
1000
500
0
*
ctrl
G6PDKD
J
glucose oxidation
(relative to normoxic WT)
1.0
0.8
0.6
0.4
0.2
0.0
*
WT
PHD1-/-
K
glutamine oxidation
(relative to normoxic WT)
1.0
0.8
0.6
0.4
0.2
0.0
*
WT
PHD1-/-

FIGURE S4: RELATED TO FIGURE 4

A, Levels of glycolytic intermediates in WT and PHD1$^{-/-}$ neurons (n = 3, p = NS). G6P, glucose-6-phosphate; F6P, fructose-6-phosphate; F1,6BP, fructose-1,6-biphosphate; PEP, phosphoenolpyruvate. **B,** G6PD mRNA expression levels (expressed as mRNA copies/10^3 copies β-actin) in WT and PHD1$^{-/-}$ neurons (n = 3, p = NS). **C,** oxPPP flux in WT neurons transduced with a lentiviral vector, expressing an empty control (ctrl) or human TIGAR (hTIGAR) (n = 4). **D,** oxPPP flux in PHD1$^{-/-}$ neurons transduced with lentiviral vectors expressing a scrambled control (ctrl) or shTIGAR (TIGAR^{KD}) (n = 5). **E-G**, Representative images of mitoSOX stained WT (E) and PHD1$^{-/-}$ neurons (F), revealing mitochondrial superoxide radical levels. Neurons were counterstained with DAPI to visualize cell nuclei. Panel G shows the quantification of mitoSOX fluorescence per cell (n = 3; p = NS; 100-200 cells per isolation were quantified). **H,** Schematic representation of the effect of silencing G6PD (shG6PD) on the PPP flux, the conversion of oxidized to reduced glutathione, and the detoxification of H_2O_2. **I,** oxPPP flux in PHD1$^{-/-}$ neurons transduced with lentiviral vectors, expressing scrambled control (ctrl) or shG6PD (G6PD^{KD}) (n = 3). **J,K,** Glucose (J) and glutamine oxidation (K), measured in hypoxic WT and PHD1$^{-/-}$ neurons (expressed relative to the values obtained in normoxic WT neurons, n = 4). All quantitative data are mean ± SEM. * $p < 0.05$.

TABLE S3: GENE EXPRESSION ANALYSIS OF ANTI-OXIDANT ENZYMES (RELATED TO FIGURE 4)

GENE	WT NEURONS	PHD1$^{-/-}$ NEURONS
Gclc	20.94 ± 1.94	25.63 ± 8.76
Gpx1	383.68 ± 77.43	398.65 ± 39.53
Gpx4	201.26 ± 16.16	231.60 ± 18.66
Prdx1	258.96 ± 43.85	241.52 ± 35.67
Prdx3	142.73 ± 36.97	131.77 ± 39.92
Prdx4	158.40 ± 57.18	154.41 ± 20.80
Sesn1	11.28 ± 1.11	12.07 ± 0.72
Sesn2	10.08 ± 2.23	10.47 ± 1.22
SOD1	655.87 ± 66.86	642.80 ± 93.91
SOD2	212.56 ± 68.75	176.86 ± 48.09

Quantitative RT-PCR data of the mRNA levels of different anti-oxidant genes in WT and PHD1$^{-/-}$ neurons in baseline conditions. Values represent number of mRNA copies/10^3 copies of *HPRT* (mean ± SEM, n = 3-6, p = NS). *Gclc*: glutamate-cystein ligase catalytic subunit; *Gpx*: glutathione peroxidase; *Prdx*: peroxiredoxin; *Sesn*: sestrin; *SOD*: superoxide dismutase.

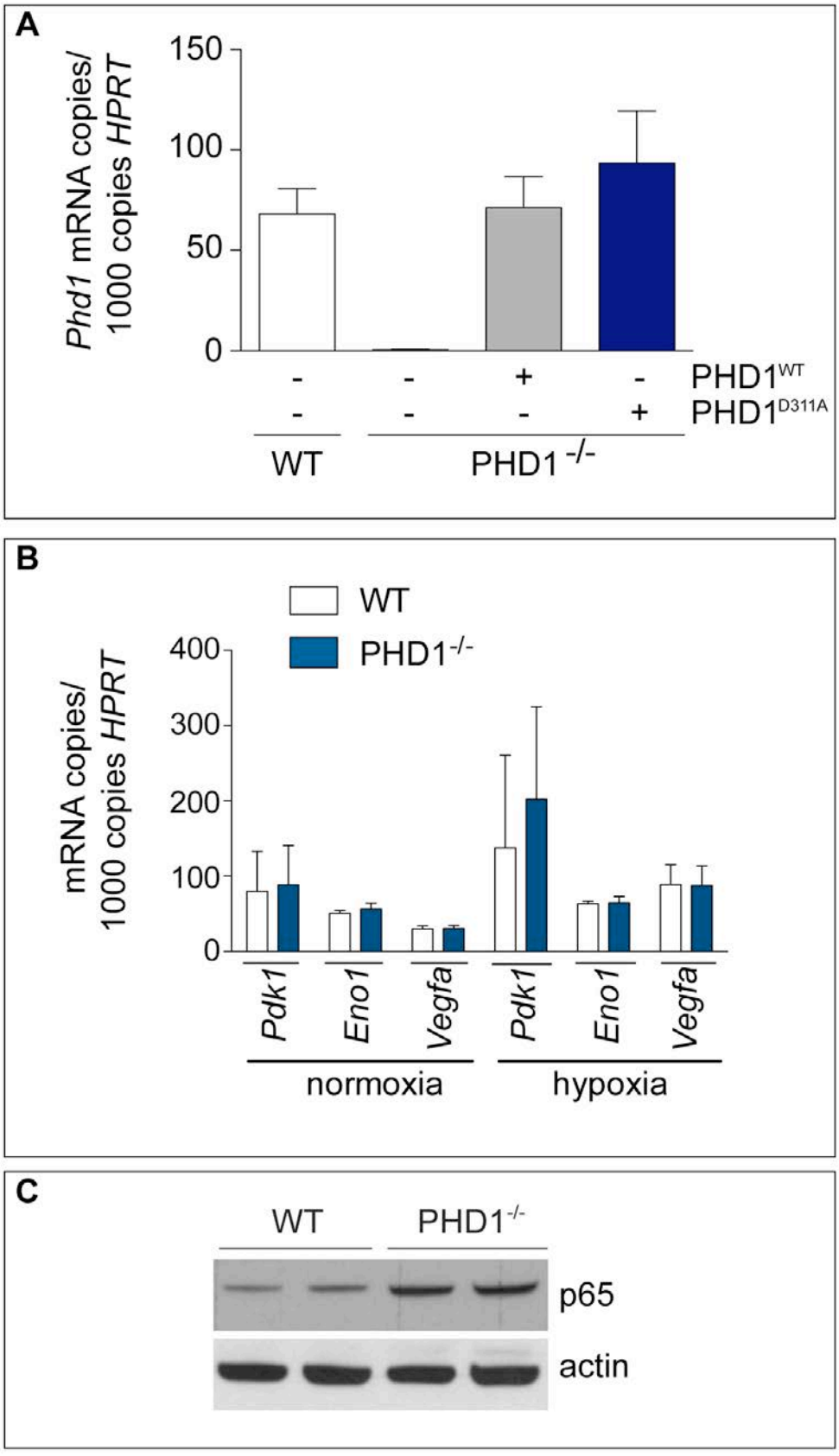
A
Phd1 mRNA copies/
1000 copies HPRT
150
100
50
0
- - + - PHD1WT
- - - + PHD1D311A
WT
PHD1 -/-
B
WT
PHD1-/-
mRNA copies/
1000 copies HPRT
400
300
200
100
0
Pdk1
Eno1
Vegfa
Pdk1
Eno1
Vegfa
normoxia
hypoxia
C
WT
PHD1-/-
p65
actin

FIGURE S5: RELATED TO FIGURE 6

A, PHD1 mRNA expression levels in control WT and PHD1$^{-/-}$ neurons with or without transduction with lentiviral vectors expressing WT PHD1 (PHD1^{WT}) or an hydroxylation-defective mutant PHD1 (PHD1^{D311A}) (n = 3). **B**, mRNA expression levels of HIF1α transcriptional targets in normoxic and hypoxic WT or PHD1$^{-/-}$ neurons (n = 3-5). *Eno1*, enolase; *Pdk1*, pyruvate dehydrogenase kinase 1; *Vegfa*, vascular endothelial growth factor A. **C**, Representative immunoblots of total p65 levels in WT and PHD1$^{-/-}$ neurons. Densitometric quantification of independent experiments (% of control β-actin): 76.6 ± 8.4% in WT and 95.9 ± 8.4% in PHD1$^{-/-}$ neurons, n = 3, $p < 0.05$). All quantitative data are mean ± SEM.

SUPPLEMENTAL EXPERIMENTAL PROCEDURES

MOUSE STRAINS USED IN THIS STUDY

PHD1$^{-/-}$ (Aragones et al., 2008), PHD2$^{lox/lox}$ (Mazzone et al., 2009) and PHD3$^{-/-}$ (Aragones et al., 2008) mice were previously reported. Given the embryonic lethality of homozygous global PHD2 deficiency (Takeda et al., 2006), neural specific PHD2 deficient mice were used, generated by intercrossing Nestin-Cre mice (Tronche et al., 1999) with PHD2$^{lox/lox}$ mice (Mazzone et al., 2009). The *Nestin*-Cre mice were on a C57Bl/6N background and were a kind gift from Dr. R. Klein (MPI, Germany). *Nestin*-Cre mice were intercrossed with PHD2$^{lox/lox}$ mice. *Nestin*-Cre^{+} PHD2$^{lox/lox}$ (PHD2^{NKO}) mice were compared with littermates *Nestin*-Cre^{-} PHD2$^{lox/lox}$ (ctrl). WT C57Bl/6N and 129S mice were obtained from the KU Leuven animal facility. For the *in vivo* experiments, only male mice, aged 8-11 weeks, littermates or age-matched mice on a pure C57Bl/6N or 129S background were used. Housing and experimental animal procedures were approved by the Institutional Animal Care and Research Advisory Committee of the University of Leuven, Belgium.

ISCHEMIC STROKE VIA PERMANENT MIDDLE CEREBRAL ARTERY OCCLUSION

Brain ischemia was induced in 8-11 weeks old male wild type and PHD1$^{-/-}$ mice using the permanent middle cerebral artery occlusion (pMCAO) model (Kuraoka et al., 2009). Both C57Bl/6N and 129S6 backgrounds were used, as indicated. Under the surgical microscope, a skin incision was made between the left orbit and tragus. The zygomatic arch was removed and temporal muscle retracted laterally. A 2-mm burr hole was made with a microdrill through the outer surface of the semitranslucent skull over the visually identified middle cerebral artery. The dura was carefully opened and the M1 branch of the MCA was exposed and ligated producing a permanent ligation of the distal middle cerebral artery. The wound was sutured and temperature was controlled by keeping the mice on a heating plate at 37 °C until they regained full consciousness. Mice were randomly assigned to treatments and the procedure was performed by an experimenter blinded for the genotypes.

HISTOLOGICAL ANALYSIS OF INFARCT SIZE

At 24 hours after ischemia, mice were euthanized and brains were removed, sliced coronally at 1 mm intervals and stained by immersion in a 2% solution of the vital dye 2,3,5-triphenyltetrazolium hydrochloride (TTC) for 30 minutes at 37 ºC. TTC will be reduced by active mitochondrial dehydrogenases, indicative of viable tissue, resulting in the formation of a deep-red product (formazan) (Bederson et al., 1986). For each coronal slice the unstained portion was delineated, and infarction area was calculated as the ratio of the unstained area (white) over the total bihemispheric area with Image J. The analysis was performed by an experimenter blinded for the genotypes and treatments.

ADHESIVE TAPE REMOVAL TEST

The performance in the adhesive tape removal test was used as a functional parameter to monitor the functional impact of the stroke as previously described (Bouet et al., 2009). Mice were trained during 7 days prior to stroke induction. A 3 mm x 4 mm piece of tape was attached to both forepaws. Time to sensation and to removal was recorded for both paws. Three separate measurements were done 1 day before stroke and at 1, 4, 8 and 11 days post-stroke. The analysis was performed by an experimenter blinded for the genotypes and treatment.

MORPHOLOGICAL AND HISTOLOGICAL ANALYSIS OF BRAIN VASCULATURE

To compare LARGE ARTERIES AND ARTERIOLES in WT and PHD1$^{-/-}$ mice, animals were perfused transcardially with saline followed by 4% PFA. Brains were dissected and post-fixed in 4% PFA overnight at 4°C, cryoprotected in sucrose 20% and embedded in optimal cutting temperature (OCT) embedding medium. Serial coronal cryosections of 10 µm thickness were incubated overnight with the primary antibody anti-αSMA-Cy3 (C6198, Sigma, 1/500). Slices were mounted with Prolong Gold + DAPI (Invitrogen). To assess VESSEL PERFUSION, WT and PHD1$^{-/-}$ mice were injected via the tail vein with fluorescein isothiocyanate (FITC)-conjugated dextran (molecular weight 2x10^6 Da, Sigma) shortly

before transcardial perfusion, and were thereafter processed for cryosectioning. Vessel perfusion after stroke was assessed by i.v. injection of fluorescein isothiocyanate (FITC)-conjugated dextran (molecular weight $2x10^6$ Da, Sigma) of the mice 2 hours after ligating the middle cerebral artery. Shortly thereafter the mice were euthanized and transcardially perfused. Coronal cryosections through the non-stroked brain or through the stroke area and corresponding contralateral cortex area were stained with Alexa568-conjugated isolectin B4 (Vector Laboratories), visualizing the vessel wall. The ratio of dextran-positive area over the isolectin-positive area reflected the perfused vessels. Visualization of the PIAL COLLATERAL CIRCULATION in WT and $PHD1^{-/-}$ mice was done via vascular corrosion casting as previously described (Krucker et al., 2006). The thoracic aorta was cannulated retrogradely and 1 ml of freshly prepared polyurethane resin (PU4ii, VasQtec) was infused into the cerebral vasculature. The PU4ii mixture was freshly prepared by adding 0.8 g of hardener (VasQtec) to PU4ii diluted in dimethylethylketone, immediately before the injection. Following resin injection, mice were anesthetized and perfused with 4% PFA. After solidification of the resin for 5 days at room temperature, brains were dissected and were repeatedly rinsed in 30% KOH. Images of the corrosion casting were captured by a Zeiss LSM 780 confocal microscope (Carl Zeiss). The number of collaterals was counted manually per hemisphere. Collaterals were defined as vessels connecting the tree of the anterior cerebral artery with the tree of the middle cerebral artery, or connecting one arteriole from the middle cerebral artery with an arteriole from the same vascular tree. All analyses were performed by an experimenter blinded for the genotypes.

MAGNETIC RESONANCE IMAGING OF PERFUSION POST-STROKE

Focal brain ischemia was induced in male 129S mice (8-10 weeks) as described before (Kuraoka et al., 2009). Mice were scanned at 2 hours and 24 hours post-surgery (anesthesia: isoflurane 1.2-1.4%, in medical air). MR images were recorded on a 9.4 T Biospec small animal MR system (20 cm horizontal bore, Bruker Biospin, Ettlingen, Germany) using a 7 cm linearly polarized resonator for transmission and an actively decoupled mouse brain surface coil for receiving (Rapid Biomedical, Rimpar, Germany).

T2w images (effective TE 50 ms; matrix 256x256; 300 µm slice thickness) were first acquired to assess the vasogenic lesion volume. Next perfusion (ASL) data were acquired from an axial slice location that covered the largest part of the T2w lesion using a FAIR approach (Kim, 1995; Kwong et al., 1995) and a RARE readout with the following specific parameters: TR 10 s, TE 5.3 ms, rare factor 72, FOV 2.5x2.5 cm, matrix 256x256, partial FT with 16 overscan, slice thickness 1 mm, inversion slab thickness 1.6 mm, 7 inversion times from 100-4000 ms, using a inversion hyperbolic secant of 14 ms (Paravison 5.1, Bruker).

Vasogenic lesion volumes were determined by manual delineation on the T2w images (Paravison 5.1). The FAIR perfusion data were first converted to quantitative perfusion images using the T1 difference method assuming an arterial T1 of 2.4s (Kober et al., 2008; Oosterlinck et al., 2011) implemented via a home-written Python (Python software foundation) scripts. Next area's with reduced perfusion were derived using an in-house developed Mevislab (Mevis Medical Solutions AG, Bremen, GE) processing pipeline using a threshold-based approach with the contra-lateral cortex as a reference region (threshold: cerebral blood flow, CBF ≤ 80%). All quantitative data are mean ±SEM.

ISOLATION AND CULTURE OF MURINE CORTICAL NEURONS

Cultures of cortical neurons were prepared as previously described (Thathiah et al., 2009). Briefly, neuron cultures from WT and PHD1$^{-/-}$ mice (both mixed Swiss/129S background) were isolated from the cortices of embryonic day 14.5 or 15.5 mice, pooled from one litter, plated on poly-D-lysine and laminin coated plates and maintained in serum-free Neurobasal media containing 25 mM glucose, supplemented with 0.5 mM glutamine and B27 supplement (all from Invitrogen). After 3 days in culture, 8 µM cytosine arabinoside (Sigma) was added to prevent non-neuronal proliferation. These cultures contained >98% MAP2^{+} neurons after 7 days in culture, as determined by staining for the glial marker GFAP, and the oligodendrocyte markers NG2 and Olig2. This fraction of contaminating non-neuronal cells (<2%) in the cultures did not differ between the two genotypes.

LENTIVIRAL TRANSDUCTIONS

Lentiviral shRNA vectors against glucose-6-phosphate dehydrogenase (G6PD), TIGAR, PHD2, PHD3, HIF-1α, HIF-2α, HIF-1β and Rel-A were ordered from the TRC 1.5 lentivirus-based shRNA library (Sigma). The shRNA ID numbers were TRCN0000041443 and TRCN0000041447 for G6PD, TRCN0000115292 and TRCN0000115294 for TIGAR, TRCN0000232222 for HIF-1α, TRCN0000082306 for HIF-2α, TRCN0000079929 and TRCN0000079931 for HIF-1β (combined), TRCN0000009740 for PHD2, TRCN0000009753 for PHD3, and TRCN0000055346 for Rel-A. A similar nonsense scrambled shRNA sequence was used as a negative control for all these experiments. Production of lentiviruses by transfection into 293T cells was as described (Carlotti et al., 2004). After 2 days in culture, the cultured neurons were exposed overnight to a multiplicity of infection (MOI) of 10 after which the medium was refreshed. Knockdown efficiency was assessed 4 days after transduction by qPCR.

To obtain overexpression of TIGAR at physiological levels, WT neurons were transduced with a lentiviral construct of human TIGAR at MOI 0.5 (Life Technologies, Mammalian Gene Collection ID4576725). Wild type PHD1 or hydroxylation-inactive mutant PHD1 were expressed in $PHD1^{-/-}$ neurons by transducing them with the corresponding lentiviral constructs at MOI 5 (McNeill et al., 2002). Neurons at 5 days in *in vitro* culture (DIV) were transfected with a tandem Tomato (tdT) expressing construct, using Lipofectamine2000 (Invitrogen), following manufacturer's instructions. To assess NF-kB promotor activity we co-transduced cells at DIV5 with a lentiviral NF-kB luciferase reporter (Cignal Lenti NFkB reporter, SABioscience, MOI 5), consisting of a tandem repeats of the NF-kB transcriptional response element and a renilla control reporter (Cignal™ Lenti TK-Renilla control, SABioscience, MOI 0.5) serving as an internal control. After 48 hours cells were lysed and luciferase and renilla enzymatic activity was measured in Microlumat LD96V Luminometer (Berthold Technologies) using the Dual Luciferase assay (Promega) as described by manufacture's instructions. The ratio of firefly over renilla luminescence represents the NF-kB promotor activity in the cell lysates.

OXYGEN-NUTRIENT DEPRIVATION ASSAY *IN VITRO*

After 7 days in culture, neurons were exposed for 2 hours to 0.1% oxygen in nutrient-deprived medium (Dullbeco's Modified Eagle's Medium (D5030, Sigma) lacking glucose, glutamine and pyruvate, supplemented with 7.5 mM $NaHCO_3$ and 5 mM HEPES (pH=7). After this period of oxygen-nutrient deprivation, neurons were re-exposed to ambient air and regular nutrient-containing culture medium (Neurobasal medium supplemented with 0.5 mM glutamine and B27 supplement minus anti-oxidants, all from Invitrogen). The lack of anti-oxidants in the medium prevented masking a neuron-intrinsic improvement of ROS detoxification, which is crucial in all neuronal cell death assays relating to oxidative stress. Neuronal cell death was quantified 24 hours later by measuring LDH release in the culture medium using the Cytotoxicity Detection Kit (Roche Applied Science). LDH release after maximal lysis of control wells (with Triton-X) was used to calculate the relative cell death. At different time-points during reperfusion, cells were harvested for GSSG/GSH measurements (see below).

METABOLIC FLUX ASSAYS

Metabolic fluxes were measured using radiolabeled tracer glucose, glutamine and lactate (all tracers were from American Radiolabeled Chemicals). Postulating that metabolic changes might account for the protective effect, all metabolic measurements were performed after 7 days in culture (7 DIV), the time at which cultures are used for the oxygen-nutrient deprivation assay. GLYCOLYSIS was measured as ^3H_2O formation using [5-^{3}H]-D-glucose as previously described (De Bock et al., 2013). Briefly, at 7 DIV, cortical neurons were incubated for 2 hours with medium containing labeled [5-^{3}H]-glucose (0.5 µCi/mmol). After this incubation period, the medium was transferred to glass vials, which were closed with rubber stoppers each containing a hanging well with a soaked (200 µl Milli-Q water) filter paper (1 cm x 6 cm) to capture the evaporated ^3H_2O. The vials were incubated for 48 hours at 37°C. Afterwards, the filter papers were transferred to scintillation vials containing 5 ml of scintillation fluid (Lumasafe 3087, Perkin Elmer) and counted with the Tri-Carb 2900TR Liquid Scintillation Analyzer (Perkin Elmer). GLUCOSE

OXIDATION was assessed as $^{14}CO_2$ formation using [6-^{14}C]-D-glucose. At 7 DIV, cortical neurons were incubated for 2 hours with medium containing labeled [6-^{14}C]-D-glucose (1 µCi/mmol). Perchloric acid ($HClO_4$) (250 µl, 3 M) was used to stop cellular metabolism and to lyse the cells. The release of intracellular CO_2 was captured by Whatman filter papers soaked in hyamine covering the lid over a period of 24 hours at room temperature. Next, the filter papers were transferred to scintillation vials and counted by the Scintillation Analyzer. OXIDATIVE PENTOSE PHOSPHATE PATHWAY (oxPPP) was measured as $^{14}CO_2$ formation using [6-^{14}C]-D-glucose ($^{14}CO_2$ formation only in the TCA cycle) and [1-^{14}C]-D-glucose ($^{14}CO_2$ formation both in the TCA cycle and the oxPPP). Cortical neurons were cultured in parallel wells and incubated with medium containing [6-^{14}C]-D-glucose (1 µCi/mmol) or medium containing [1-^{14}C]-D-glucose (1 µCi/mmol). Released $^{14}CO_2$ was captured in a similar manner as described above for glucose oxidation. The [6-^{14}C]-glucose flux was then subtracted from the [1-^{14}C]-glucose flux. The relative contribution of the oxPPP flux to glucose metabolism was assessed by including glycolytic flux in the relative flux measurements as described before (Ashcroft et al., 1972). GLUTAMINE OXIDATION was measured as $^{14}CO_2$ formation using [U-^{14}C]-glutamine. Cortical neurons were incubated with medium containing [U-^{14}C]-glutamine for 2 hours. Cells were lysed with $HClO_4$ and $^{14}CO_2$ was captured in hyamine-soaked filter papers. LACTATE OXIDATION was measured in a similar way as $^{14}CO_2$ formation after incubation with medium containing [U-^{14}C]-lactate. OXYGEN CONSUMPTION RATE (OCR) was measured using the extracellular flux analyzer XF24 (Seahorse Bioscience Inc.). Cortical neurons were plated and grown for 7 days in a Seahorse XF24 tissue culture plate. At 7 DIV, the oxygen consumption rate was measured over a period of 2 minutes. In baseline conditions, 5 consecutive measurements of OCR are done. Next, oligomycin, a blocker of ATP synthase is injected at 12 µM (concentration in well 1.2 µM). The drop in OCR reflects the oxygen consumption serving ATP production. In parallel wells, dinitrophenol (DNP), a mitochondrial uncoupler is injected at 1 mM (concentration in well 100 µM). This forces neurons to use their maximal mitochondrial capacity in order to preserve the mitochondrial membrane potential. The increase in OCR reflects the reserve capacity of mitochondria. As a second injection,

Antimycin-A is added at 10 µM (concentration in well 1 µM), a complex III inhibitor. This shuts down the electron transport chain activity abolishing the mitochondrial oxygen consumption, allowing the calculation of baseline mitochondrial respiration (OCR_{BAS}). The residual OCR corresponds to the non-mitochondrial oxygen consumption. All mitochondrial inhibitors were from Sigma. HYPOXIA EXPOSURE: To assess metabolic fluxes in hypoxia, we exposed neuronal cultures to 0.1 % O_2 during the 2 hours incubation with radiolabeled tracer glucose and glutamine.

G6PD ACTIVITY MEASUREMENT

G6PD activity was measured in neuronal lysates obtained from 7 DIV cultures, using the colorimetric Glucose 6 Phosphatase Assay Kit (Abcam) following manufacturer's instructions.

ASSESSMENT OF REACTIVE OXYGEN SPECIES *IN VITRO*

The scavenging capacity of reactive oxygen species (ROS) was measured by assessing the detoxification rate of H_2O_2 after loading the cells (7 DIV) with 10 µM 5-(and-6)-chloromethyl-2',7'-dichlorodihydrofluorescein diacetate (CM-H_2-DCFDA, Molecular Probes, Invitrogen). CM-H_2-DCFDA is metabolized by intracellular esterases to a non-fluorescent product, which is oxidized to the fluorescent product CM-DCF, by H_2O_2. The dye was washed away and cells were exposed to 100 µM H_2O_2. Fluorescence was measured over time with a fluorescent plate reader. Mitochondria-localized superoxide radicals (O_2^-) were measured using the mitochondria-targeted, O2-sensitive fluorogenic probe mitoSOX Red (Molecular Probes, Invitrogen). Briefly, WT and PHD1$^{-/-}$ neurons (7 DIV) were loaded with mitoSOX Red (5 µM) for 10 minutes at 37°C and 5% CO_2. Following fixation with 4 % PFA, mitoSOX Red fluorescence (Absorption/emission maxima: 510/580 nm) was detected using a Leica DMI6000B epifluorescence microscope (Leica, Manheim, Germany). Average fluorescent intensity and cell nuclei numbers were measured by Leica LASAF-MMAF morphometric analysis (Metamorph, Leica Microsystems, Mannheim, Germany).

ASSESSMENT OF INTRACELLULAR SODIUM CONCENTRATION

WT and PHD1$^{-/-}$ neurons were cultured on coverslips and at 7-8 DIV loaded with 10 µM SBFI-AM (Invitrogen) and 0.06% Pluronic F-127 (Invitrogen) for 45 min at 37°C. The intracellular Na^+ concentration ($[Na^+]_i$) was monitored using SBFI-based microfluorimetry. Changes in $[Na^+]_i$ were monitored on an Olympus IX81 inverted microscope through the ratio (R) of fluorescence measured upon alternating illumination at 340 and 380 nm using an MT-10 illumination system and the *xcellence pro* software (Olympus, Planegg, Germany) at room temperature. To convert R to absolute $[Na^+]_i$ values, an *in situ* calibration was performed as described earlier (Diarra et al., 2001). Briefly, cells were treated with 5 µM gramicidin D (Sigma), a channel-forming ionophore, and subsequently perfused with solutions containing 10 mM HEPES (pH 7.4), 1 mM $MgCl_2$, 2 mM $CaCl_2$ and increasing concentrations of NaCl (0, 5, 10, 50, 100, 150 mM), supplemented with KCl such that NaCl and KCl concentration always sums up to 150 mM. From these data, a calibration curve (R *vs* $[Na^+]$) was constructed and fitted with the equation:

$$[Na^+]_i = K_m \times [(R-R_{min})/(R_{max}-R)].$$

The deduced parameters (K_m, R_{min} and R_{max}) were then used to calculate $[Na^+]_i$ from experimental R values.

The standard extracellular solution for $[Na^+]_i$ measurements contained 150 mM NaCl, 5 mM KCl, 1 mM $MgCl_2$, 2 mM $CaCl_2$, 10 mM glucose and 10 mM HEPES (pH 7.4). After equilibration for 10 minutes in this solution, R was monitored during 2 minutes, yielding a value for the basal $[Na^+]_i$. Subsequently, KCl was omitted from the standard extracellular solution during 10 minutes, thus inhibiting Na^+ extrusion via Na^+/K^+-ATPases. This resulted in a robust rise in $[Na^+]_i$, which reflects basal Na^+ influx via Na^+-dependent transporters and ion channels. Finally, the cells were again perfused with the standard, K^+-containing solution, resulting in a gradual restoration of the basal $[Na^+]_i$ due to Na^+ extrusion by the Na^+/K^+-ATPases.

ANALYSIS OF PROTEIN AND RNA SYNTHESIS

Protein synthesis: cortical neurons were labeled with 50 µM Click-IT L-Homopropargylglycine (HPG, Molecular Probes) for 24 hours to allow incorporation during protein synthesis. After fixation of the cells with 4% PFA, the incorporated HPG was detected by a 'click reaction' with Alexa-647 according to the manufacturer's instructions. *RNA synthesis*: cortical neurons were labeled with 50 µM Click-IT ethinyl-uridine (EU, Molecular Probes) for 24 hours to allow incorporation during RNA synthesis. After fixation of the cells with 4% PFA, the incorporated EU was detected by a 'click it reaction' with Alexa-647 according to the manufacturer's instructions. HPG or EU signal intensities and cell nuclei numbers were measured by Leica LASAF-MMAF morphometric analysis (Metamorph, Leica Microsystems, Mannheim, Germany).

LC-MS ANALYSIS OF GLUTATHIONE (GSH-GSSG ASSAY)

Cultured neurons were extracted in 100 µl 5% TCA and cortex tissue from stroke area and corresponding contralateral area were extracted in 500 µl 5% TCA. Following extraction, the lysate was transferred to a fresh Eppendorf tube and 100 µl mq H_2O was added and the mixture centrifuged for 10 minutes at 20,000 x g. The supernatant was transferred to a fresh vial and 100 µl, was injected onto an Acquity UPLC HSS T3 column (2.1 x 100 mm, particle size 1.8 µm, cat # 186003539, Waters) using an Ultimate 3000 UPLC (Thermo Scientific) in-line connected to a Q-Exactive OrbiTRAP mass spectrometer (Thermo Scientific). The column was thermostated at 37 °C. A linear gradient was carried out using solvent A (0.05% formic acid) and solvent B (60% methanol, 0.05% formic acid). Briefly, 1% solvent B was maintained for 10 minutes, then increased to 100% B at 12 minutes and kept at 100 % B for 3 minutes (t =15 minutes). The gradient was returned to 1% solvent B at 16 minutes and allowed to re-equilibrate until 21 minutes. The flow rate was kept constant at 250 µl/minute. Elution of GSH and GSSG was observed at respectively 3 and 6 minutes. The mass spec operated in targeted SIM mode following ions with m/z 308.09108 (GSH, z=1) and 613.15979 (GSSG, z=1) eluting between 1 and 10 minutes of the gradient. The mass spectrometer was set to positive ion mode, AGC target of 1 e6

ions and a maximum injection time of 50 ms. The sheath gas flow was set at 35, the auxiliary gas flow rate at 10. The spray voltage was used at 3.00 kV and the capillary was heated at 350 °C. Auxiliary gas heater temperature was placed at 300 °C.

GC-MS ANALYSIS OF GLUCOSE CONSUMPTION

At 5 DIV, culture medium of WT and PHD1$^{-/-}$ neurons was changed to equal amounts of fresh medium. Twenty four hours later, medium samples were collected. Glucose content was assessed by MS. Glucose consumption was determined as the difference between blank samples (medium 24 hours without cells) and the medium obtained from WT and PHD1$^{-/-}$ neuronal cultures. Values were corrected by cell number (protein content). To 50 µl of medium 450 µl of methanol (Ultrapure, Sigma-Aldrich) at -80°C was added. The solution was put for 2 hours at -80°C and supernatant was collected following a centrifugation step at 4°C for 15 min at 20,000 x g. Next, the supernatant was dried using a vacuum centrifuge. To the dried fractions 50 µl of hydroxylamine hydrochloride solution (Sigma-Aldrich, Bornem, Belgium) was added, the reaction was carried out for 60 min at 90°C, samples were cooled down and 100 uL of propionic anhydride (Sigma) was added. The reaction lasted for 30 min at 60°C. Next, samples were dried and fractions were dissolved in 100 uL ethyl acetate and transferred to appropriate Agilent glass vials with conical inserts. GC-MS analyses were performed using an Agilent 7890A GC equipped with a HP-5 ms 5% Phenyl Methyl Silox (30 m - 0.25 mm i.d. - 0.25 µm; Agilent Technologies, Santa Clara, California, USA) capillary column, interfaced with a triple quadruple tandem mass spectrometer (Agilent 7000B, Agilent Technologies) operating under ionization by electron impact at 70 eV. The injection port, interface and ion source temperatures were kept at 230 °C. Temperature of the quadrupoles was maintained at 150°C. The injection volume was 1 µl, and samples were injected at 1:75 split ratio. Helium flow was kept constant at 1 ml/min. The temperature of the column started at 80 °C for 1 min and increased to 280 °C at 20 °C/min, and held for 3 min. Next, column regeneration was carried out for 3 min at 325°C. The GC/MS/MS analyses were performed in Single Ion Monitoring (SIM) scanning for the m/z 370,15.

LC-MS ANALYSIS OF GLYCOLYTIC INTERMEDIATES

The polar metabolites were extracted using a cold two-phase methanol-water-chloroform extraction (Fendt et al., 2013; Schoors et al., 2015). The dried metabolite samples were resuspended in 60% acetonitrile and transferred to LC-MS vials. Measurements were performed using a Dionex UltiMate 3000 LC System (Thermo Scientific) in-line connected to a Q-Exactive Orbitrap mass spectrometer (Thermo Scientific). 15 ul of sample was injected and loaded onto a SeQuant ZIC/ pHILIC Polymeric column (Merck Millipore). A linear gradient was carried out starting with 84% solvent A (95-5 acetonitrile-H2O, 2mM ammoniumacetate pH 9.3) and 16% solvent B (2 mM ammoniumacetate pH 9.3). From 2 to 29 minutes the gradient changed to 75% B and was kept at 75% until 34 min. Next a decrease to 16% B was carried out to 42min and then 16% B was maintained until 58 min. The solvent was used at a flow rate of 100 ul/min, the columns temperature was kept constant at 25 degrees Celsius. The mass spectrometer operated in negative ion mode, settings of the HESI probe were as follows: sheath gas flow rate at 25, auxiliary gas flow rate at 5 (at a temperature of 260 degrees Celsius). Spray voltage was set at 4.8 kV, temperature of the capillary at 300 degrees Celsius and S-lens RF level at 50. Both a full scan (resolution of 35.000 and scan range of m/z 50-1050) as well as a targeted SIM method focusing on ions from glycolytic intermediates was applied. Data collection (abundance and 13C isotopic incorporation) was performed using Xcalibur software (Thermo Scientific).

HPLC ANALYSIS OF ENERGY CHARGE

Cells were harvested in 100 µl ice cold 0.4 M perchloric acid supplemented with 0.5 mM EDTA. pH was adjusted by adding 100 µl of 2 M K_2CO3. One hundred µl of the mixture was injected onto an Agilent 1260 HPLC equipped with a C18-Symmetry column (150 x 4.6 mm; 5 mm) (Waters), thermostated at 22.5 °C. Flow rate was kept constant at 1 ml/min. A linear gradient using solvent A (50 mM NaH_2PO4, 4 mM tetrabutylammonium, adjusted to pH 5.0 using H_2SO4) and solvent B (50 mM NaH_2PO4, 4 mM

tetrabutylammonium, 30% CH_3CN, adjusted to pH 5.0 using H_2SO4) was accomplished as follows: 95% A for 2 minutes, from 2 to 25 minutes linear increase to 100% B, from 25 to 27 minutes isocratic at 100% B, from 27 to 29 minutes linear gradient to 95% A and finally from 29 to 35 minutes at 95% A. Detection of ATP, ADP and AMP occurred at 259 nm. The energy charge is calculated as ([ATP] + ½ [ADP] / [ATP] + [ADP] + [AMP]).

IMMUNOCYTOCHEMISTRY, HISTOCHEMISTRY AND MORPHOMETRIC ANALYSIS

Cortical neurons grown on Willco-Dish glass bottom dishes (Ibidi) were fixed after 7 days in culture with PFA 4% for 10 minutes. After permeabilization for 10 minutes in 0.25% Triton and blocking 30 for minutes with 10% pre-immune serum, the cells were incubated overnight with the appropriate primary antibodies. The following antibodies were used: anti-TOMM20 (ab56783, Abcam; 1/200), anti-MAP2 (M3696, Sigma, 1/500), anti-GFAP (G3893, Sigma, 1/500), anti-NG2 (AB5320, Chemicon, 1/200), anti-Olig2 (AB9610, Chemicon, 1/20,000). The next day, the cultures were washed and incubated with the appropriate fluorescently conjugated secondary antibody (Alexa-568 or Alexa-488, Molecular Probes, Invitrogen). Fluorescence imaging was performed using Zeiss LSM 780 confocal microscope (Zeiss, Germany) or Leica DMI6000B epifluorescence microscope (Leica, Germany). Signal positive areas were quantified using the FiJI / NIH Image J software package / AxioVision morphometric analysis software (Carl Zeiss, Munich, Germany) with in-house developed macros. Quantification of arborization of tdT-transfected neurons was performed by the module for Sholl analysis in FiJI software. Nissl staining on brain sections was performed using standard protocols. Bright fields imaging was performed using a Leica DMI6000B epifluorescence microscope (Leica, Germany). Quantification of cortical thickness and lateral extension were performed using FiJI software. All quantifications were performed by researchers blinded for the genotype.

RNA, DNA AND PROTEIN ANALYSIS

RNA LEVEL ANALYSIS*:* Total RNA was extracted from cultured cortical neurons using the RNeasy microkit (Qiagen), and reverse transcribed using the Quantitect Reverse

Transcription kit (Qiagen) according to the manufacturer's instructions. Total RNA was extracted from dissected brain tissue using Trizol-chloroform extraction. After tissue homogenization with Trizol, chloroform was added to separate the aqueous phase. After centrifugation and addition of ethanol, samples underwent a RNA clean-up on a RNeasy mini column (Qiagen 74104) with DNAse I treatment (Invitrogen 12185010). Gene expression analysis was performed by Taqman quantitative RT-PCR, using premade primer sets (Applied Biosystems or IDT). Expression levels were quantified relative to the expression level of housekeeping genes (β-actin or HPRT). Primers and probes ID numbers are available upon request. MITOCHONDRIAL DNA CONTENT: For mitochondrial DNA copy measurement, total DNA was extracted from cell lysates. The amount of mitochondrial DNA relative to nuclear genomic DNA was determined by quantitative PCR using homemade primers for the genic sequences of *cytochrome b* (mitochondrial, MIT) and *RPL13A* (nuclear, NC). Forward, reverse and probe sequences were: NC FOR2 5'-aga cct gaa gag gct tcg cta a-3'; NC REV2 5'-cag ctt gcg ggt caa gct-3'; NC probe 5'-FAM-cca ccg tcc ctt cca gct acc atc cta-TAMRA-3'; and MIT FOR 5'-ttg atc aac gga cca agt tac c-3'; MIT REV 5'-cgt tga aca aac gaa cca tta ata g-3'; MIT probe 5'-FAM-aca att agg gtt tac gac ctc gat gtt gga t-TAMRA-3'. PROTEIN EXPRESSION (WESTERN BLOT ANALYSIS): Protein extraction and immunoblot analysis were performed using a modified Laemli sample buffer (125 mM Tris-HCl, pH 6.8 buffer containing 2% SDS and 10% glycerol) in the presence of protease and phosphatase inhibitors (Roche). Nuclear protein extraction was done by using the NEPER kit according to manufacturer's instructions. Lysates were separated by SDS-PAGE under reducing conditions, transferred to a nitrocellulose membrane (Life Technologies), and analyzed by immunoblotting. Primary antibodies used were goat anti-HIF1α (AF1935, R&D Systems, 1:200), goat anti-HIF2α (AF2997, R&D Systems, 1:200), rabbit anti-PHD2 (NB100-2219, Abcam, 1:1000), rabbit anti-PHD3 (1088-100, Abcam, 1:1000), rabbit anti-p65 (No. 3033 Cellsignaling, 1:1000). Equal loading was verified by incubation with rabbit anti-β-actin (13E5; No. 4970, Cell signaling), mouse anti-α-tubulin (Sigma, 1:10000) or rabbit anti-lamin A/C (No. 2032, Cell Signaling). Appropriate secondary antibodies were HRP-conjugated (Dako or Cell signaling). Signal was detected

using the ECL system (Amersham Biosciences, GE Healthcare) according to the manufacturer's instructions.

IN VIVO INFUSION OF 1,2-^{13}C GLUCOSE

SURGICAL CATHETERIZATION OF THE RIGHT JUGULAR VEIN: Mice were anesthetized with 1% isoflurane and a catheter was placed into the right jugular vein. A small incision between the shoulder blades was made and the catheter was exteriorized at the back of the mouse and connected to an antenna part, which enables conscious handling of the mouse during infusion. The tubing was flushed with heparinized saline directly after the surgery and 3 days later (Ayala et al., 2006). Animals were individually housed after surgery, and painkillers were administered (Carprofen, 5 mg/kg body weight subcutaneous) during surgery and one day after. INFUSION WITH ^{13}C LABELED GLUCOSE AND TISSUE PROCESSING: Five days after surgery, [1,2-^{13}C]-labeled glucose (99% enriched; Buchem) was infused in awake, freely moving mice. Morning fasted mice (6 hours) were subjected to a continuous infusion of 0.03 mg ^{13}C labeled glucose per gram body weight per minute during 6 hours (yielding a final ^{13}C plasma glucose enrichment of 64 ± 12%). Subsequently, the mice were sacrificed by cervical dislocation, blood was collected and different brain regions were dissected within less than 5 minutes and immediately frozen using a liquid nitrogen cooled Biosqueezer (Biospec Products). The tissue was weighed (10-15 mg) and pulverized (Cryomill, Retsch) under liquid nitrogen conditions. The polar metabolites were extracted using a cold two-phase methanol-water-chloroform extraction (Fendt et al., 2013; Schoors et al., 2015). The dried metabolite samples were resuspended in 60% acetonitrile and transferred to LC-MS vials. Metabolite measurements were performed using a Dionex UltiMate 3000 LC System (Thermo Scientific) coupled to a Q Exactive Orbitrap mass spectrometer (Thermo Scientific) operated in negative mode. Fifteen µl of sample was injected on a SeQuant ZIC/ pHILIC Polymeric column (Merck Millipore). The solvent was used at a flow rate of of 100 µl/min and was composed of an acetonitrile / ammonium acetate (pH 9.3, 2 mM) mixture. Data collection was performed using Xcalibur software (Thermo Scientific). Blood glucose enrichment in the infused mice was measured as

described above in the section on GC-MS analysis of glucose consumption. Pilot experiments in cultured neurons incubated with [1,2-^{13}C]-glucose showed that the percentage of M+1 labeling in lactate and alanine, which is commonly used to reflect the PPP activity, was not affected by PHD1 deficiency. Nevertheless, PHD1$^{-/-}$ neurons show enhanced flux as measured by the differential $^{14}CO_2$ production from [1-^{14}C]-glucose and [6-^{14}C]-glucose, which reflects the oxidative branch of the PPP. These data suggest that the enhanced flux through the oxidative branch does not result in a subsequent increase of the non-oxidative PPP flux towards glycolysis. We therefore quantified the ratio of the fractional M+1 *vs* M+2 labeling of pentose-5-phosphate (P5P), as this is indicative for the relative importance of the oxPPP *vs* non-oxPPP. While also M+4 can arise from a net of exchange flux of the non-oxidative PPP towards P5P, the M+4 enrichment was substantially lower than the M+2 enrichment. We therefore considered only the M+1 and M+2 enrichment in P5P to characterized the relative importance of the oxidative vs non-oxidative PPP.

ICV DELIVERY OF ANTISENSE OLIGONUCLEOTIDES AGAINST PHD1 IN STROKE

Oligonucleotides directed against murine PHD1 were designed and purified by Isis Pharmaceuticals. These antisense oligonucleotides (ASOs) are directed against the regions within the coding region and 5' and 3' untranslated region of the PHD1 mRNA. After binding to complementary target RNA through Watson-Crick base-pairing, the target RNA will be degraded by RNaseH-mediated RNA degradation. Additional modifications consisting of a *O*-(2-methoxy)ethyl substitution at the 2' position and phosphorothioate substitution were created to increase the resistance of the ASOs against nuclease activity and in this way promote their stability. Three top ASOs of 20 nucleotides long were selected for further investigation. Knockdown efficiency was tested in cultured cortical neurons. At 2 DIV, cortical neurons were exposed to 0.5 µM and 1 µM of anti-PHD1 ASOs. To ensure correct dosing, the absorbance at 260 nm was regularly measured in the stock solution. An oligonucleotide that targets murine MALAT-1 (Metastasis associated lung adenocarcinoma transcript; non coding RNA in the nucleus) was used as control ASO.

Similar to MALAT-1 knockout mice (Zhang et al., 2012), anti-MALAT1 ASO does not induce a phenotype in the central nervous system and is well tolerated in neurons (C.F.B., G.H., unpublished data). At 7 DIV, cortical neurons were harvested for RNA extraction and qPCR for PHD1, PHD2 and PHD3.

One out of the three ASOs with the highest efficiency and specificity was selected for further *in vivo* studies. A dose of 75 µg ASO/day (selected in pilot experiments) was infused into the left lateral ventricle of male C57Bl/6N mice (age 7-8 weeks), using Alzet® osmotic pumps (model 2004, Cupertino), connected with a catheter to a brain infusion cannula. The brain infusion assembly was filled with a solution, containing the ASO diluted in artificial CSF (aCSF) or with aCSF alone (saline control). For the *in vivo* studies both saline and a non-RNAase H active ASO to human huntingtin was used as control. After anesthesia with ketamine and xylazine, the osmotic pump was subcutaneously inserted in the midscapular area on the back of the mouse. After exposing the skull through a midline sagittal incision, a hole was drilled through the skull, and the cannula placed using the following stereotactic coordinates: 0 mm posterior and 1 mm lateral to bregma, and 2 mm deep from skull surface. After 10 days of infusion, brains were harvested from a series of test mice to assess knockdown efficiency. Two weeks after the infusion, pMCAO was performed. There was no difference in stroke size between saline and control ASO groups, demonstrating that injection of an ASO *per se* did not cause additional effects that would influence stroke outcome.

SUPPLEMENTAL REFERENCES

Ashcroft, S.J., Weerasinghe, L.C., Bassett, J.M., and Randle, P.J. (1972). The pentose cycle and insulin release in mouse pancreatic islets. Biochem J *126*, 525-532.

Carlotti, F., Bazuine, M., Kekarainen, T., Seppen, J., Pognonec, P., Maassen, J.A., and Hoeben, R.C. (2004). Lentiviral vectors efficiently transduce quiescent mature 3T3-L1 adipocytes. Mol Ther *9*, 209-217.

De Bock, K., Georgiadou, M., Schoors, S., Kuchnio, A., Wong, B.W., Cantelmo, A.R., Quaegebeur, A., Ghesquiere, B., Cauwenberghs, S., Eelen, G.*, et al.* (2013). Role of PFKFB3-Driven Glycolysis in Vessel Sprouting. Cell *154*, 651-663.

Diarra, A., Sheldon, C., and Church, J. (2001). In situ calibration and [H+] sensitivity of the fluorescent Na+ indicator SBFI. Am J Physiol Cell Physiol *280*, C1623-1633.

Fendt, S.M., Bell, E.L., Keibler, M.A., Olenchock, B.A., Mayers, J.R., Wasylenko, T.M., Vokes, N.I., Guarente, L., Vander Heiden, M.G., and Stephanopoulos, G. (2013). Reductive glutamine metabolism is a function of the alpha-ketoglutarate to citrate ratio in cells. Nat Commun *4*, 2236.

Kim, S.G. (1995). Quantification of relative cerebral blood flow change by flow-sensitive alternating inversion recovery (FAIR) technique: application to functional mapping. Magn Reson Med *34*, 293-301.

Kober, F., Duhamel, G., and Cozzone, P.J. (2008). Experimental comparison of four FAIR arterial spin labeling techniques for quantification of mouse cerebral blood flow at 4.7 T. NMR Biomed *21*, 781-792.

Kwong, K.K., Chesler, D.A., Weisskoff, R.M., Donahue, K.M., Davis, T.L., Ostergaard, L., Campbell, T.A., and Rosen, B.R. (1995). MR perfusion studies with T1-weighted echo planar imaging. Magn Reson Med *34*, 878-887.

Oosterlinck, W.W., Dresselaers, T., Geldhof, V., Van Santvoort, A., Robberecht, W., Herijgers, P., and Himmelreich, U. (2011). Response of mouse brain perfusion to hypo- and hyperventilation measured by arterial spin labeling. Magn Reson Med *66*, 802-811.

Tronche, F., Kellendonk, C., Kretz, O., Gass, P., Anlag, K., Orban, P.C., Bock, R., Klein, R., and Schutz, G. (1999). Disruption of the glucocorticoid receptor gene in the nervous system results in reduced anxiety. Nat Genet *23*, 99-103.

Zhang, B., Arun, G., Mao, Y.S., Lazar, Z., Hung, G., Bhattacharjee, G., Xiao, X., Booth, C.J., Wu, J., Zhang, C.*, et al.* (2012). The lncRNA Malat1 is dispensable for mouse development but its transcription plays a cis-regulatory role in the adult. Cell Rep *2*, 111-123.